

ISTANBUL TECHNICAL UNIVERSITY ★ EURASIA INSTITUTE OF EARTH SCIENCE

**MODELING THE STRUCTURAL EVOLUTION OF THE LOW-ANGLE
DETACHMENT FAULTS IN WESTERN ANATOLIA BACK ARC SYSTEM**



M.Sc. THESIS

Ömer BODUR

Department of Solid Earth Science

Geodynamics Programme

JUNE 2019

ISTANBUL TECHNICAL UNIVERSITY ★ EURASIA INSTITUTE OF EARTH SCIENCE

**MODELING THE STRUCTURAL EVOLUTION OF THE LOW-ANGLE
DETACHMENT FAULTS IN WESTERN ANATOLIA BACK ARC SYSTEM**

M.Sc. THESIS

**Ömer BODUR
(602171002)**

Department of Solid Earth Science

Geodynamics Programme

Thesis Advisor: Assoc. Prof. Dr. Oğuz Hakan GÖĞÜŞ

HAZİRAN 2019

İSTANBUL TEKNİK ÜNİVERSİTESİ ★ AVRASYA YER BİLİMLERİ ENSTİTÜSÜ

**BATI ANADOLU YAY ARDI HAVZASINDA GELİŞEN DÜŞÜK AÇILI
NORMAL FAYLARIN GELİŞİMİNİN MODELLENMESİ**

YÜKSEK LİSANS TEZİ

Ömer BODUR

602171002

Katı Yerbilimleri Anabilim Dalı

Jeodinamik Programı

Tez Danışmanı: Doçent Dr. Oğuz Hakan GÖĞÜŞ

HAZİRAN 2019

Ömer BODUR, a M.Sc. student of İTÜ Graduate School of Science Engineering and Technology student ID 602171002, successfully defended the thesis entitled “MODELING THE STRUCTURAL EVOLUTION OF THE LOW-ANGLE DETACHMENT FAULTS IN WESTERN ANATOLIA BACK ARC SYSTEM”, which he prepared after fulfilling the requirements specified in the associated legislations, before the jury whose signatures are below.

Thesis Advisor : **Assoc. Prof. Dr. Oğuz Hakan GÖĞÜŞ**

Istanbul Technical University

Jury Members : **Prof. Dr. Hans THYBO**

Istanbul Technical University

Dr. Derya GÜRER

University of Queensland

Date of Submission : 3 May 2019

Date of Defense : 10 June 2019





To my family,

FOREWORD

First, I would like to thank my thesis supervisor Assoc. Prof. Dr. Oğuz Hakan Göğüş for his continuous guidance, support and patience during my masters. I am very grateful to have agreed to work with him as a master student. My thesis, presentations and posters were not possible without him.

I would like to thank Sascha Brune and Anne Glerum for allowing us to use the cluster at GFZ Potsdam and for patiently answering my endless questions about the ASPECT program that we used.

I would like to thank Hasan Sözbilir, who has always supported us in the geology of the region and shared his experience with us.

I want to thank Deniz Ural for his work on the visualization part of the models, what he taught me and his friendship.

I am very happy to share a room with my friends Barış Şen, Açelya Ballı and Uğurcan Çetiner. They have always been supportive and encouraging.

I appreciate to thank my dear friends Gözde Kuran, Ceyhun Erman, and Ahmet Gezgin for their continuous encouragement and motivation.

Finally, I would like to thank my father İbrahim Kemal Bodur and my mother Figan Bodur to their unrequited love and support to me during my whole life. I owe my family everything I've achieved in my life, including this master thesis.

June 2019

Ömer BODUR



TABLE OF CONTENTS

	<u>Page</u>
FOREWORD	xi
TABLE OF CONTENTS	xiii
ABBREVIATIONS	xv
SYMBOLS	xvii
LIST OF TABLES	xix
LIST OF FIGURES	xxi
SUMMARY	xxiii
ÖZET	xxv
1. INTRODUCTION	1
1.1. Low Angle Detachment Faults and Exhumation of Metamorphic Core Complexes.....	1
1.2. Rolling-Hinge Mechanism.....	3
2. EXTENSIONAL TECTONICS IN WESTERN ANATOLIA	7
2.1. Geological Framework	8
2.2. Geophysical Studies.....	11
2.3. Thermochronological Studies	14
2.4. Objective of the Study	16
3. METHODOLOGY	17
3.1. Explanation of the Numerical Model.....	17
3.2. Model Setup.....	18
3.3. Measurement of Fault Angles.....	22
4. MODEL RESULTS	23
4.1. Reference Model.....	23
4.1.1. Extension rate effect.....	26
4.1.2. Friction strain weakening factor of the upper crust effect.....	30
5. MODEL RESULTS AGAINST OBSERVATIONS	37
REFERENCES	41
CURRICULUM VITAE	45



ABBREVIATIONS

LAB	: Lithosphere Asthenosphere Boundary
Ma	: Million Years Ago
MOHO	: Mohorovicic Discontinuity
My	: Million Years Later





SYMBOLS

κ	: Thermal conductivity
τ	: Shear stress
C	: Cohesion
σ	: Normal stress
\mathbf{g}	: Gravity vector
t	: Time
u, v	: Displacement Vector Components
T	: Temperature
C_p	: Heat capacity
H	: Rate of internal heat production
α	: Thermal expansion coefficient
ρ	: Density
θ	: Angle of friction
$\dot{\epsilon}$: Strain rate
A	: Viscosity parameter
n	: Power exponent
Q	: Activation energy
R	: Ideal gas constant



LIST OF TABLES

	<u>Page</u>
Table 3.1 : Model parameters for the different layers of the reference model. Other parameters are assumed to be constant. But their sensitivity on the results may be tested in future experiments.	19
Table 4.1: Fault angles for different extension rates depending on time. Strain weakening factor and the internal angle of friction remained the same value.....	30
Table 4.2: Fault angles for different strain weakening factor for the upper crust values depending on time. Extension rates and the internal angle of friction remained the same value.....	35



LIST OF FIGURES

	<u>Page</u>
Figure 1.1 : Conceptual model of detachment faults (Wernicke & Axen, 1988).....	1
Figure 1.2 : Frequency of earthquakes versus dip, both nodal planes, from Jackson & White (1989).....	2
Figure 1.3: Ideas about the development of the detachment faults. (a) After Miller, Gans and Garing (1983); (b) after Bartley and Wernicke (1984); (c) after Buck (1988). Not drawn to scale. (Platt, Behr, & Cooper, 2014).	3
Figure 1.4: Cartoons showing the development of the detachment fault (Seyitoglu, Tekeli, Çemen, Şen, & Işık, 2002).	5
Figure 2.1: Tectonic map of the Anatolia and red circled region is the research area. Right top of the figure shows GPS velocities and orientation map with respect to Eurasia fixed reference frame. (Nocquet, 2012).	7
Figure 2.2: a) Simplified geological map shows location of main tectonic units and main structural units in western Anatolia. b) Synthetic cross section of the region with the structural investigations of this study(Çifçi, Pamukçu, Çoruh, Çopur, & Sözbilir, 2011; Lips, Cassard, Sözbilir, Yılmaz, & Wijbrans, 2001).	9
Figure 2.3: Conceptual bivergent rolling-hinge mechanism for central Menderes Massif (Gessner et al., 2001).	10
Figure 2.4: Seismic reflection studies for the Büyük Menderes detachment fault. a) N-S trending, seismic profile in association with the sequence stratigraphic unit, b) E-W trending, seismic profile in association with the sequence stratigraphic units. The red lines represent the main graben bounding fault (Simply modified from Çifçi, Pamukçu, Çoruh, Çopur, & Sözbilir (2011)).....	12
Figure 2.5: The interpreted seismic profiles were depth converted to link with the surface geology. Transverse geological cross-sections showing the geometry of the Gediz Graben. Both of the seismic profiles are trending with N-S direction. The red lines represent the main graben bounding fault (Simply modified from Çiftçi & Bozkurt (2010)).....	13
Figure 2.6: The red line shows the Moho depth that observed with the receiver function studies in the Bornova Flish Zone, Menderes Massif and the Lycian Nappes. Moho depth is 25-30 km beneath the Menderes Massif and its undulating structure seem (Karabulut et al., 2013).	14
Figure 2.7: Fission-track data for the western Anatolia. Numbers with the dashed lines are the cooling ages (Gessner et al., 2001).	15
Figure 2.8 : Thermochronological results from Nilus et al., (2019) and show that the cooling ages of the rocks.	15

Figure 3.1 : Model setup for the extensional tectonics in the western Anatolia and the strength and the strain softening profiles. Orange: Upper crust, Purple: Lower crust, Red: Lithospheric mantle, Blue: Asthenosphere.	21
Figure 3.2: Cartoon shows the measurement of the angles of the faults at different time step due to rolling-hinge mechanism.	22
Figure 4.1: Fault development of model with extension 1 cm/yr. (A) after 2 My., (B) after 6 My., (C) after 14 My., (D) after 20 My. The top of the model represents the upper crust, purple areas represent the lower crust. Regions where the strain rate is red colored deformation is high.	24
Figure 4.2 : 22 My. after model started and the last time step of the reference model.	25
Figure 4.3: Fault development of model with extension 1 cm/yr. (A) after 2 My., (B) after 6 My., (C) after 14 My., (D) after 20 My. The top of the model represents the upper crust, purple areas represent the lower crust. Regions where the strain rate is red colored deformation is high.	27
Figure 4.4: Fault development of model with extension 3 cm/yr. (A) after 2 My., (B) after 6 My., (C) after 14 My., (D) after 20 My. The top of the model represents the upper crust, purple areas represent the lower crust. Regions where the strain rate is red colored deformation is high.	28
Figure 4.5: Fault development of model with extension 4 cm/yr. (A) after 2 My., (B) after 6 My., (C) after 14 My.. The top of the model represents the upper crust, purple areas represent the lower crust. Regions where the strain rate is red colored deformation is high.	29
Figure 4.6: Fault development of model with the friction weakening factor of the upper crust is 0.1. (A) after 2 My., (B) after 6 My., (C) after 14 My., (D) after 20 My. The top of the model represents the upper crust, purple areas represent the lower crust. Regions where the strain rate is red colored deformation is high.	31
Figure 4.7: Fault development of model with the friction weakening factor of the upper crust is 0.2. (A) after 2 My., (B) after 6 My., (C) after 14 My., (D) after 20 My. The top of the model represents the upper crust, purple areas represent the lower crust. Regions where the strain rate is red colored deformation is high.	32
Figure 4.8: Fault development of model with the friction weakening factor of the upper crust is 0.4. (A) after 2 My., (B) after 6 My., (C) after 14 My., (D) after 20 My. The top of the model represents the upper crust, purple areas represent the lower crust. Regions where the strain rate is red colored deformation is high.	33
Figure 4.9: Fault development of model with the friction weakening factor of the upper crust is 0.5. (A) after 2 My., (B) after 6 My., (C) after 14 My., (D) after 20 My. The top of the model represents the upper crust, purple areas represent the lower crust. Regions where the strain rate is red colored deformation is high.	34
Figure 5.1 : (a) The reference model at $t = 22$ My and the observed seismic reflection profiles for the Gediz and Büyük Menderes detachment faults (Çiftçi et al., 2011; Çiftçi & Bozkurt, 2010). (b) Observed Moho topography from receiver function studies (Karabulut et al., 2013).....	38
Figure 5.2 : The reference model at $t = 2$ My and fission-track study for the initial fault angles (Gessner et al., 2001).....	39

MODELING THE STRUCTURAL EVOLUTION OF THE LOW-ANGLE DETACHMENT FAULTS IN WESTERN ANATOLIA BACK ARC SYSTEM

SUMMARY

Extensional tectonics in the western Anatolia-Aegean region feature exhumation of the metamorphic core complexes that is accommodated by low angle normal (detachment) fault systems. Specifically, the central Menderes massif contains two symmetrically developed outward facing (Gediz and Büyük Menderes) detachment faults, which accommodated large scale displacements. Additionally, there are many younger high-angle normal faults in conjunction with the initiation of extension and synextensional magmatism since the Early Miocene. The standard fault mechanical theory does not allow such orientations, the occurrence of these faults at low angle and the seismicity on them are still not well-understood. Here, we investigate the evolution of the normal fault systems on lithospheric scale using thermomechanical forward models. We employ the numerical finite element code ASPECT to compute the viscoplastic deformation within a model domain that is 500 km wide and 165 km deep. The initial condition of our model is designed to reproduce the first-order lithospheric structure at the onset of Western Anatolia extension approximately 20 million years ago and consists of an upper crust (25 km thick) with wet quartzite rheology, a lower crust (25 km thick) with wet anorthite rheology, and a mantle lithosphere (30 km thick) with dry olivine rheology. We conduct two model suits where we investigate the impact of key parameters within a plausible range: (1) we vary the extension velocities imposed on the margins of the model boundary from $V_{ext} = 1-4$ cm/year full rate. (2) we vary the friction strain weakening factor of the upper crust ($f_c = 0.1$ to 0.5). Our models show that these two parameters directly control the initial dip angle and development of the normal faults. We find that major faults are formed initially at $50-52^\circ$ dip but evolve towards shallower dipping angles, $10-15^\circ$, because of the isostatic adjustment due to thinning/exhumation of the crust. The sequentially tilted faults on where slip can no longer be accommodated are abandoned and left behind as inactive low angle fault surfaces. Basin ward migration of newer fault is formed in the hanging wall to accommodate strain. The tectonic evolution of the central Menderes region is best reproduced in our reference model with a friction strain weakening factor of 0.2 and an extension rate of $V_{ext} = 3$ cm/yr. Namely, this model agrees well with the detachment faults shallowing dip angles, outward facing faults and symmetry with respect to the central Menderes massif. In addition, the exhumed massif has a dome shaped structure and the distance to one another (80 km) is comparable to those of Western Anatolia. Also, high angle normal faults are formed above the detachment faults, typical for Gediz and Büyük Menderes grabens. When the friction strain weakening factor of the upper crust and extension rates are changed, differences in these structural elements are observed. We conclude that our reference model supports the two rolling-hinge detachment system separated by elongated metamorphic domes with fold axes perpendicular to the direction of extension.



BATI ANADOLU YAY ARDI HAVZASINDAKİ DÜŞÜK AÇILI NORMAL FAYLARIN GELİŞİMİNİN MODELLENMESİ

ÖZET

Ege ve Batı Anadolu bölgesinin Helenik yitim zonunun geri çekilmeye başlamasının etkisi ile birlikte genişlemekte olduğu uzun zamandır bilinmektedir. Yapılan GPS çalışmalarından elde edilen bilgilere göre, bölgenin yıllık olarak yaklaşık 2 ile 3 santimetre genişlediği bilinmektedir. Bölgede yapılan birçok çalışma olup, geniş alanlarda görülen sismik anomaliler, horst-grabenler, sıyrılma fayları, magmatizma ve içerdiği metamorfik çekirdek kompleksler nedeni ile birçok araştırmacının dikkatini çekmiştir. Özellikle Menderes Masifi'nde, büyük ölçekli yer değiştirmeleri barındıran birbirine simetrik olarak gelişmiş iki sıyrılma fayı (Gediz ve Büyük Menderes) yer almaktadır. Ayrıca, erken Miyosen'den bu yana genişlemenin ve magmatizmanın başlaması ile bağlantılı olarak çok sayıda genç yüksek açılı normal fay da görülmektedir.

Standart fay teorisi fayların düşük açıda oluşmasına olanak sağlamaz, sadece 45° üzerinde oluşabileceğini söyler. Bu nedenle fayların oluşum mekanizması, bugünkü açılara nasıl ulaştıkları ve sismisiteleri hala tartışmalıdır. Bu konuda da oldukça fazla çalışma ve önerilmiş teoriler bulunmaktadır. Yapılan sismisite çalışmalarına bakıldığında 30° ve altında olan fayların sismisitesinin çok az, 15° ve altındaki faylarda ise neredeyse hiç olmadığı görülür. Dolayısı ile bölgedeki yüksek sismisitenin, sıyrılma faylarının üzerinde gelişmiş olan yüksek açılı normal faylardan dolayı kaynaklandığı söylenebilir.

Bölgede yapılan alıcı fonksiyon çalışmalarında, Batı Anadolu'nun altında Moho derinliğinin 25-30 kilometre olduğu söylenebilir. Buna ek olarak, aynı zamanda Moho'nun ondulasyonlu bir yapıya sahip olduğu görülür. Yapılan fizyon iz tarihlendirme çalışmalarında, bölgedeki düşük açılı sıyrılma faylarının, yüksek açılı olarak oluştuğu ve devam eden zamanda açılarının düştüğü söylenmiştir ve oluşum açılarının yaklaşık olarak 50° ve 60° olduğu ileri sürülmüştür.

Batı Anadolu için önerilen model iki kollu Rolling-hinge mekanizmasıdır. Bu mekanizmaya göre, açılmaya bağlı olarak birbirine simetrik olarak gelişen iki yüksek açılı fay gelişmektedir. Açılmanın ilerleyen aşamalarında izostatik dengeye cevap olarak yükselen taban bloğu ile yüksek açılı normal faylar zamanla düşük açılı normal faylara dönmektedir. Ek olarak, yeni yüksek açılı normal faylar bu düşük açılı normal fayların üzerinde oluşmaktadır. Yükselmeye bağlı olarak derinlerdeki metamorfik

kayalar da yüzeye çıkmaktadır. Dolayısı ile önerilen iki kollu rolling-hinge mekanizması, Batı Anadolu'da yer alan sıyrılma faylarının ve metamorfik çekirdek kompleksin oluşumunun ve gelişiminin anlaşılmasında oldukça açıklayıcıdır.

Bu çalışmada, litosferik ölçekte termo-mekanik modeller kullanarak normal fay sistemlerinin gelişim mekanizması açıklanmaktadır. Çalışmada model genişliği 500 km, derinliği 165 km seçilmiş ve visko-plastik deformasyonu hesaplamak için sayısal sonlu elemanlar kodu olan ASPECT kullanılmıştır. Model sağ ve sol köşelerinden eşit miktarda açılmaya uğratılmıştır ve bu açılmaların toplamı, toplam açılma hızına eşittir. Çıkan malzemelerin yerine, modelin alt sınırından astenosfer girişi yapılmıştır.

Modellerin başlangıçtaki durumu, yaklaşık 20 milyon yıl önce Batı Anadolu ile uyumlu litosferik yapıyı yeniden üretecek şekilde tasarlanmıştır. Bu modelde, 25 km kalınlığında bir üst kabuk (ıslak kuvarsit), 25 km kalınlığında bir alt kabuk (ıslak anortit) ve 30 km kalınlığında bir manto litosferi (kuru olivin) oluşturulmuştur. Toplamda 50 kilometrelik kalın bir kabuk kullanılmasının nedeni, açılmadan önce bölgenin bir çarpışma kuşağında yer almasıdır. 30 kilometrelik ince manto litosferinin kullanılmasının nedeni ise, çarpışmadan sonra kalınlaşan manto litosferinin bir kısmının gravitasyonel etkiler altında kalarak koptuğunun söylenmesidir.

Anahtar parametrelerin uygun bir aralıktaki etkisini araştırdığımız iki model takımı belirlenmiştir. Bunlar: (1) Modellerdeki açılma hızlarını $V_{ext} = 1-4$ cm/yıl arasında, (2) Üst kabukta zayıflama faktörünün 0.1 ile 0.5 arasında değişen parametrelerden oluşturulmuştur. Modelleme çalışmasında üst kabuk için kırılğan, diğer katmanlar için sünek davranış kullanılmıştır. Herhangi bir zayıf zon ya da daha önceden oluşmuş bir fay kullanılmamış olup, sadece genişleme tektoniğinin fay gelişimindeki etkisine bakılmıştır.

Modellerde bu iki parametrenin doğrudan fayların oluşum açılarını ve gelişimlerini kontrol ettiği görülmüştür. Modelin ortasında birbirine simetrik olarak gelişen yüksek açılı normal faylar gözlemlenmiştir. Bu ana faylar $50-52^\circ$ ile oluşup, kabuğun açılmasına bağlı olarak gelişen izostatik dengeye cevap olarak yükselen alt kabuğa bağlı olarak, açıları $15-20^\circ$ 'ye kadar düşmektedir. İlerleyen zaman adımlarında bu sıyrılma faylarının üzerinde yeni yüksek açılı normal faylar gelişmektedir. Menderes Masifi'nin tektonik evrimine en uygun olarak, sürtünme katsayısının 0.2 ve açılma hızının $V_{ext} = 3$ cm/yıl olduğu model referans model olarak seçilmiştir. Bu modelde, Menderes Masifi'ndeki sıyrılma faylarının bugünkü eğim açılarına ve simetrilerine uyum sağladığı ve yükselen masifteki dom yapısı ile Batı Anadolu ile örtüştüğü görülmüştür. Yapılan sismik yansıma çalışmalarında da görüldüğü gibi, ana sıyrılma fayının üzerinde yeni gelişen yüksek açılı normal faylar modellerde de gözlenmektedir. Ayrıca Moho derinliği ve ondulasyonlu yapısı, yapılan alıcı fonksiyon çalışmaları ile uyum içinde bulunmuştur. Bunlara ek olarak, başlangıç açıları yapılan fizyon iz tarihlendirme çalışmalarına uygundur. Referans model, Batı Anadolu için önerilen, kıvrım eksenleri açılma doğrultusuna dik olan metamorfik domlar ile ayrılan iki taraflı 'rolling hinge' mekanizmasını desteklemektedir. Şu ana kadar

yapılan modellerde, zayıflama faktörünün fayların simetrisi ya da asimetrisini kontrol eden ana mekanizma olarak bulunmamıştır. İleride yapılacak olan yeni modeller, bölgenin ve sıyrıma faylarının anlaşılmasında bize daha da yardımcı olacaktır.





1. INTRODUCTION

1.1. Low Angle Detachment Faults and Exhumation of Metamorphic Core Complexes

The detachment faults were first discovered in the Basin and Range province (Armstrong, 1972; Longwell, 1945; Wernicke, 1981) and have since been the origin of the faults are most debated issues. Detachment faults are gently dipping (commonly less than 30°), generally domed structure, due to broad magnitude slip (normally 10-50 km). Detachments may underlie thousands of kilometers and, most large-displacement detachments are revealing in dome structures with diameter 10-30 km that are mirrored in the topography. Generally, the footwall of the detachments is topographically high and domed. These dome structures are formed as a response to isostatic adjustment of the footwall. During the rise of the footwall of the detachment fault in this response, the deeper metamorphic rocks exhume at the surface. Removal

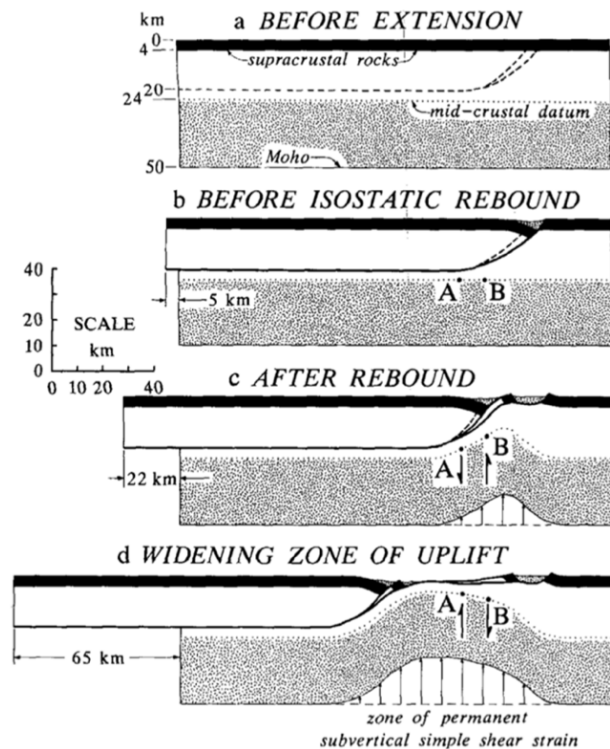


Figure 1.1 : Conceptual model of detachment faults (Wernicke & Axen, 1988).

of the hanging-wall generates buoyancy force (Buck, 1988; Wernicke & Axen, 1988) and it must be compensated with materials of crustal density.

The occurrence of these faults and the seismicity on them are still not well-understood. The standard fault mechanism theory suggests the faults that have less than 30° angle cannot slip. According to the earthquake data from different locations (Greece, western Turkey, Italy, the Gulf of Suez, Tibet, NE China, Mongolia, East Africa, and the western U.S.A.), it is seen that the earthquakes mostly occur at faults that have a dip angle between 30° and 60° (Jackson & White, 1989). Considering the activity of the faults at various angles, the theories proposing that the detachment faults are initiated with low-angle are inadequate for explaining the exhumation of the metamorphic core complexes. Without the fault activity, the core complexes cannot exhume at the surface.

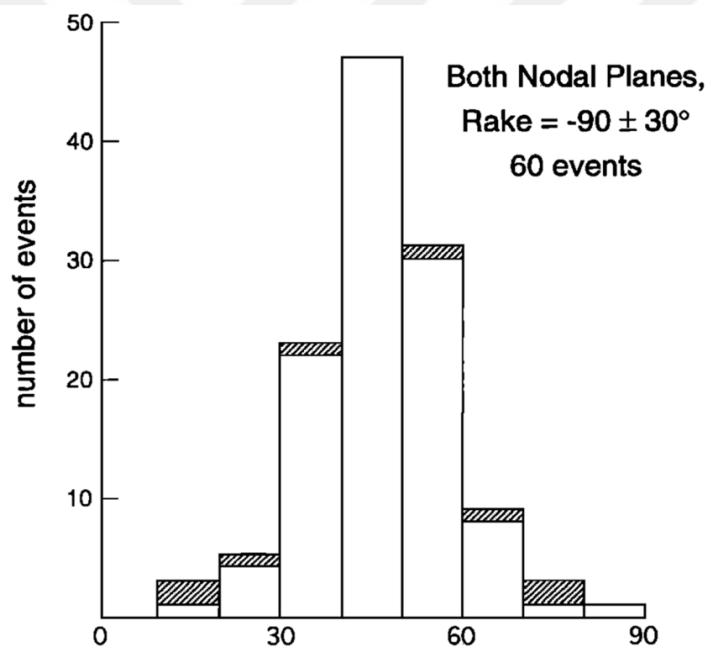


Figure 1.2 : Frequency of earthquakes versus dip, both nodal planes, from Jackson & White (1989)

Because of the standard fault mechanical theory does not allow low-angle orientations (Anderson, 1905), different theories have been proposed for the evolution of the detachment faults. According to Miller et al. (1983), detachment is located at brittle-ductile transition as a horizontal boundary, separating ductile thinning below of brittle faulting zone (Fig. 1.3.a). They estimated detachment exhuming towards the surface because of the thinning of the brittle layer, but they realized that the fault accumulated

short displacement in the process. Moreover, in their theory detachment may never break the surface during its activity. Otherwise, Bartley and Wernicke (1984) proposed that detachment is formed initially as a low-angle normal fault and cutting through the crust and the surface. Furthermore, the average dip angle of the fault is about 30° , with 80 km displacement (Fig. 1.3.b.). Another theory by Buck (1988), Davis and Lister (1988) and Wernicke and Axen (1988), is that flat-lying detachment rotated initially high angle to a low-angle by exhumation of the footwall as a response to isostatic rebound (Fig. 1.3.c.).

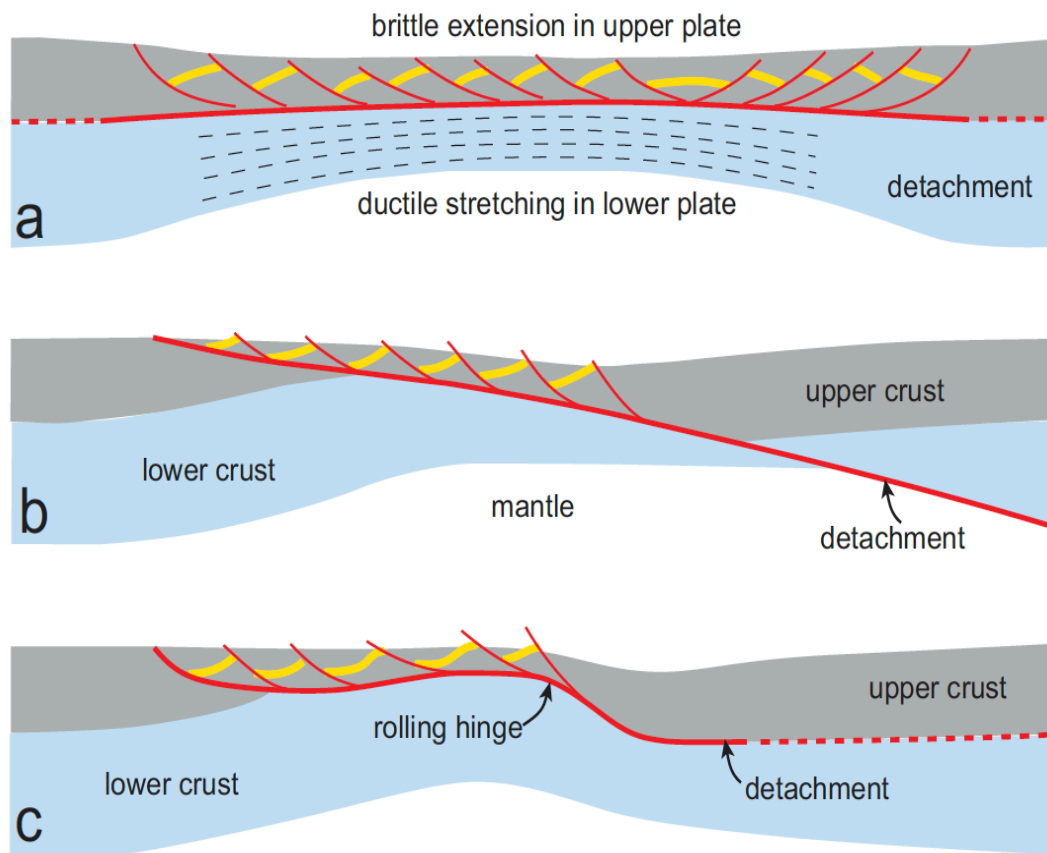


Figure 1.3: Ideas about the development of the detachment faults. **(a)** After Miller, Gans and Garing (1983); **(b)** after Bartley and Wernicke (1984); **(c)** after Buck (1988). Not drawn to scale. (Platt, Behr, & Cooper, 2014).

1.2. Rolling-Hinge Mechanism

The rolling-hinge mechanism is suggested for the development of the low-angle detachment faults and proposed that isostatic rebound during the unloading by slip on normal faults will rotate the footwall from an initially steep orientation into the horizontal position (Wernicke & Axen, 1988). The active part of the fault stays steeply

dipping, but as the footwall rocks reach at the surface and they tilt into a subhorizontal orientation (Lavie, Buck, & Poliakov, 1999). Footwall of steep normal fault is deformed by flexural uplift because active fault plane comes too flat accommodate further brittle strain, new faults form in hanging-wall (Gessner et al., 2001). The Andersonian theory and seismicity data are clarified with the formation of detachment faults furthermore, this theory does not require active slip on low-angle faults. Rolling-hinge mechanism implies that rocks in the footwall of the normal fault roll around a hinge close to the surface with a gentle dip. This theory helps to solve mechanical problem about the initiation of the low-angle normal faults moreover, it defines the rotation of the high-angle normal faults. As the extension continues, new high-angle normal faults form near that previous fault during time. This model dynamically proposed that the differential loading caused by motion on a normal fault up to a point is supported from the extending lithosphere. This process is repeated as the extension proceed. The angle of the detachment fault is low at near (15° - 20°) the surface and high angle when it goes deeper (45° - 50°).

Detachments in core complexes are distinguished principally with their sufficient displacement to exhume rocks from below the brittle-ductile transition. Active normal faults with a dip angle of less than 30° have mechanical problems because the shear stress on the fault plane has to be considerably less than frictional resistance ($\mu = 0.6$ – 0.8). Although a number of events are documented (Abbott et al., 1997; Hreinsdóttir & Bennett, 2009; Rigo et al., 1996), seismicity of the low-angle normal faults is relatively poor (Jackson, 2008).

The mechanical problem of the slip on low-angle normal faults has been answered in recent years with comprehension that most brittle faults can move under low shear stresses. The mechanical problem of the slip on low-angle normal faults has been answered in recent years with comprehension that most brittle faults can move under low shear stresses (Townend, 2006). A normal fault could slip at a dip of 10° degrees or less with a friction coefficient of 0.1 additionally, this also explains that the low of seismicity on the low-angle normal faults (Carpenter, Saffer, & Marone, 2015).

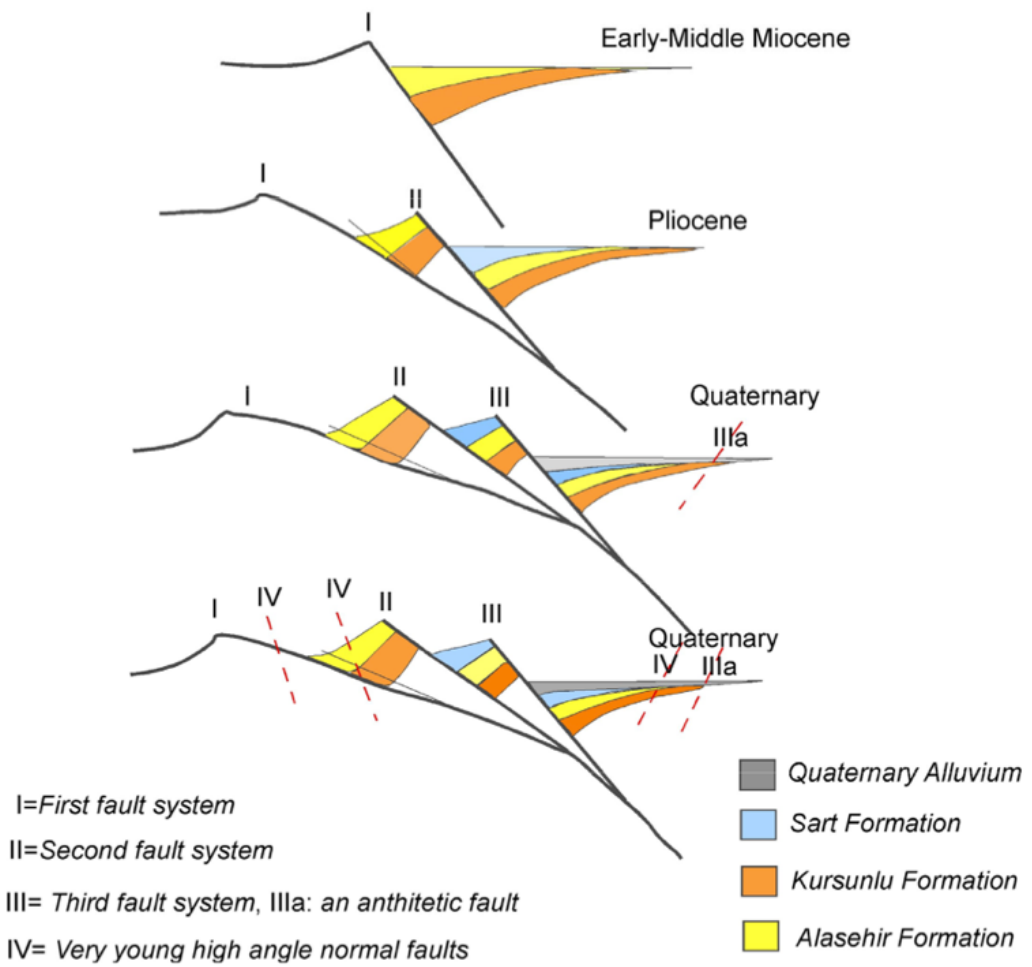


Figure 1.4: Cartoons showing the development of the detachment fault (Seyitoglu, Tekeli, Çemen, Şen, & Işık, 2002).



2. EXTENSIONAL TECTONICS IN WESTERN ANATOLIA

Western Anatolia is part of the Aegean extensional tectonic province, which is located in an active convergent zone between Eurasian and African plates. This province is one of the most seismically active and rapidly deforming part of the Alpine-Himalayan orogenic belt furthermore, the Aegean region has been deformed by the N-S oriented lithospheric scale extensional tectonics approximately since latest Oligocene–Early Miocene (~25 Ma.). Also, the area is currently under the influence of slab-pull forces by subduction of the African Plate beneath the southern part of Anatolian Plate and the dextral slip on the North Anatolian Fault System. According to the data obtained from GPS studies, the extension rate of the area is approximately 2-3 cm/yr.

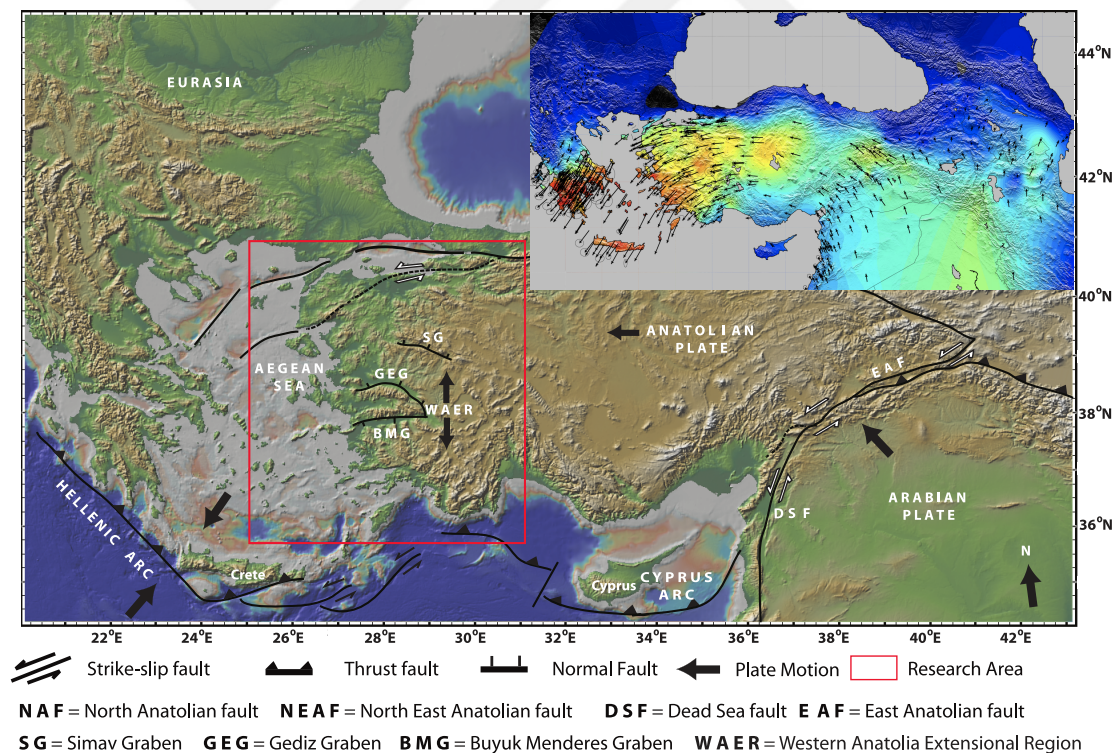


Figure 2.1: Tectonic map of the Anatolia and red circled region is the research area. Right top of the figure shows GPS velocities and orientation map with respect to Eurasia fixed reference frame. (Nocquet, 2012).

There are three main theories for caused extension in the western Anatolia; the first theory suggests that the collision between the Arabian platform and the Anatolian plate

at east side cause this extension (Dewey & Sengor, 1979). The second theory is proposed that the region locates at Alpine-Himalayan orogenic belt and during this collision lithosphere becomes thick and under the gravitational forces it led to extension (Seyitoğlu & Scott, 1996). The third and probably the most effective one is the retreat of the Hellenic subduction system (Jolivet & Brun, 2010). This subduction system started at Rhodope massif approximately 25 million years ago and during that time it retreated almost 500 kilometers. With the effect of this retreat, an extension started in the Aegean and western Anatolia.

Gediz and Büyük Menderes grabens (E-W trending) are the most prominent features of western Turkey and they take apart the Menderes Massif that is one of the largest core complexes of the World (Erdin Bozkurt & Sözbilir, 2004). Extensional tectonics in the western Anatolia-Aegean region feature exhumation of the metamorphic core complexes that is accommodated by low angle normal (detachment) fault systems (Erdin Bozkurt & Sözbilir, 2004; Emre & Sözbilir, 1997; Yılmaz et al., 2008). Specifically, the central Menderes massif contains two symmetrically developed outward facing (Gediz and Büyük Menderes) detachment faults, which accommodated large scale displacements.

2.1. Geological Framework

The graben systems subdivided three submassifs; a northern and central submassifs (Ödemiş-Kiraz submassif), and a southern submassif (the Çine submassif). The Menderes Massif is on the edge of İzmir-Ankara suture in the north and unmetamorphosed sequences of the Lycian Nappes in the south.

The Çine massif consists of a gneissic composite basement distinguished by amphibolite to granulite facies meta-sediment enclaves, and the southern part of the gneiss sequence is characterized by a well-known extensional ductile shear-zone (E. Bozkurt & Park, 1994; E. Bozkurt, Winchester, & Park, 1995; Hetzel & Reischmann, 1996). The activity of this shear zone that separates greenschist facies schist and marbles in the hanging-wall to felsic gneisses in the footwall, has been concluded to Eocene time.

The northern and central submassifs are generally consisted of schists and marbles of varying metamorphic grades (Hetzl, Romer, Candan, & Passchier, 1998). Sözbilir and Emre (1996) supposed that basal contact of the gneiss had formed as a thrust fault

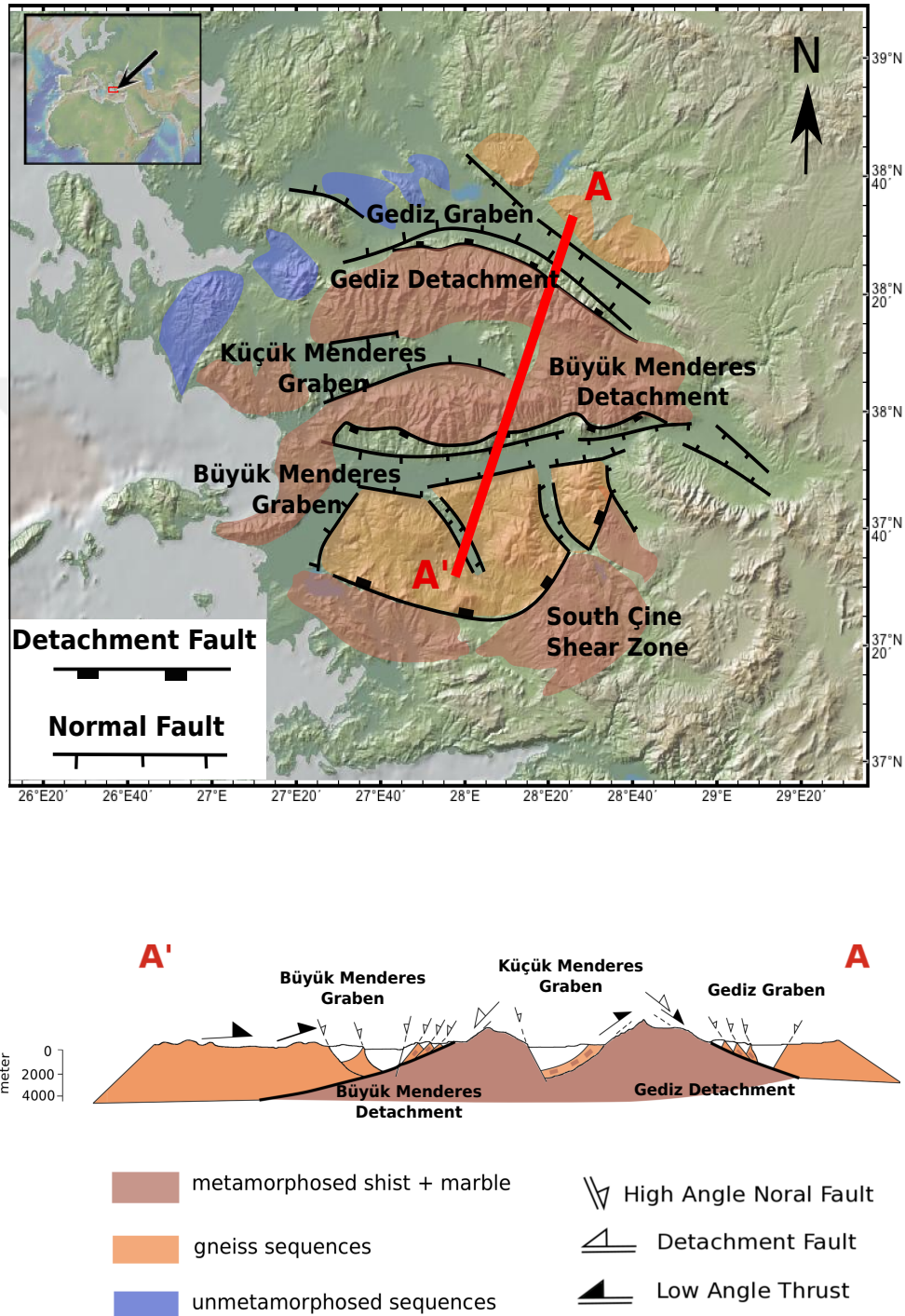


Figure 2.2: a) Simplified geological map shows location of main tectonic units and main structural units in western Anatolia. b) Synthetic cross section of the region with the structural investigations of this study (Çifçi, Pamukçu, Çoruh, Çopur, & Sözbilir, 2011; Lips, Cassard, Sözbilir, Yilmaz, & Wijbrans, 2001).

because of compressional tectonics from Eocene-Oligocene in Aegean region. After that collision, fault reactivated as a detachment fault system in Miocene.

Tectonic denudation of the Menders Massif in the Miocene is controlled by the development and activity of the Gediz detachment (Koçyiğit, Yusufoglu, & Bozkurt, 1999). Additionally, there are many younger high-angle normal faults in conjunction with the initiation of extension and synextensional magmatism since the Early Miocene (Aldanmaz, Pearce, Thirlwall, & Mitchell, 2000). The high-angle normal faults also controlled the development of the Küçük Menderes graben in the central part of the Menderes Massif (Akçay, Özkan, Moon, & Scott, 1996; Lips et al., 2001).

Proposed theory for western Anatolia is bivergent rolling-hinge mechanism. Depending on the extension, there are two high-angle normal faults in the right and the left sections of the model. When the extension progresses, the footwall of the model rises as a response to isostatic rebound depending on the unloading so, the flat-lying detachments were rotated from a high-angle to low-angle orientation. Thus, the newer high-angle normal faults are formed in conjunction with these detachment faults. During this uplift, the lower metamorphic rocks become to the surface. This two-sided rolling hinge mechanism helps to understand the development of the detachment faults and also the exhumation of the metamorphic core complex that located in the western Anatolia.

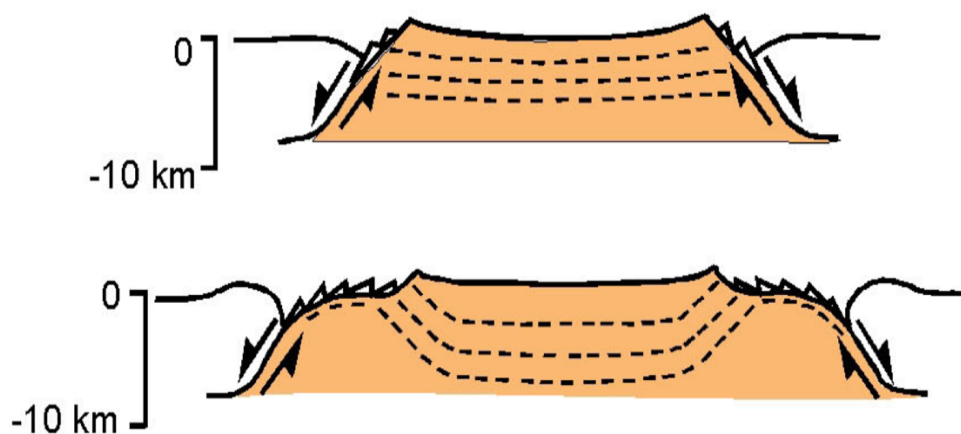


Figure 2.3: Conceptual bivergent rolling-hinge mechanism for central Menderes Massif (Gessner et al., 2001).

2.2. Geophysical Studies

The Büyük Menderes detachment fault was first mapped by Emre and Sözbilir (1997) for a re-activated thrust fault (Lips et al., 2001). This fault was explained as a thrust along which the older high-grade gneisses were brought over the younger schists during the Eocene contractional in the area. Nevertheless, Gessner et al. (2001) interpreted this surface as a low-angle normal fault. Also, it is suggested that the Büyük Menderes detachment is characterized by semiductile to brittle fault behavior (Lips et al., 2001).

Two N-S trending strike-slip faults (Nazilli and North of Kuyucak) act as accommodation or cross faults in the northern margin of the Büyük Menderes graben. E-W trending high-angle normal faults are South-dipping high-angle normal faults that have formed step-wise topography along this graben and three major structural blocks have been tilted against the fault plane because of this topography. The blocks are younger near the basin and the youngest one forms the boundary between the alluvium and all of the older units.

The zone of detachment is about 10 km deep, where the listric faults turn horizontally. Thus, a main zone of the detachment must have developed during the rifting time. This zone signifies the transition from brittle to ductile behavior in a hot and wet crust during the rifting period.

The deepest detachment fault governs the region according to the N-S compiled seismic and geological data, moreover the other faults operate on it. This fault separates the sedimentary and the metamorphic rocks and shapes boundary.

The southern part of the Gediz graben is structurally complicated by two group of faults: (1) low-angle detachment fault that is a currently inactive and (2) high-angle normal faults. The high-angle faults are younger towards the basin (Cohen, Dart, Akyüz, & Barka, 1995). An important field relationship is the detachment fault representing the contact between metamorphic basement and sedimentary cover. High-angle normal faults dissect the detachment and result in back-tilting of the detachment.

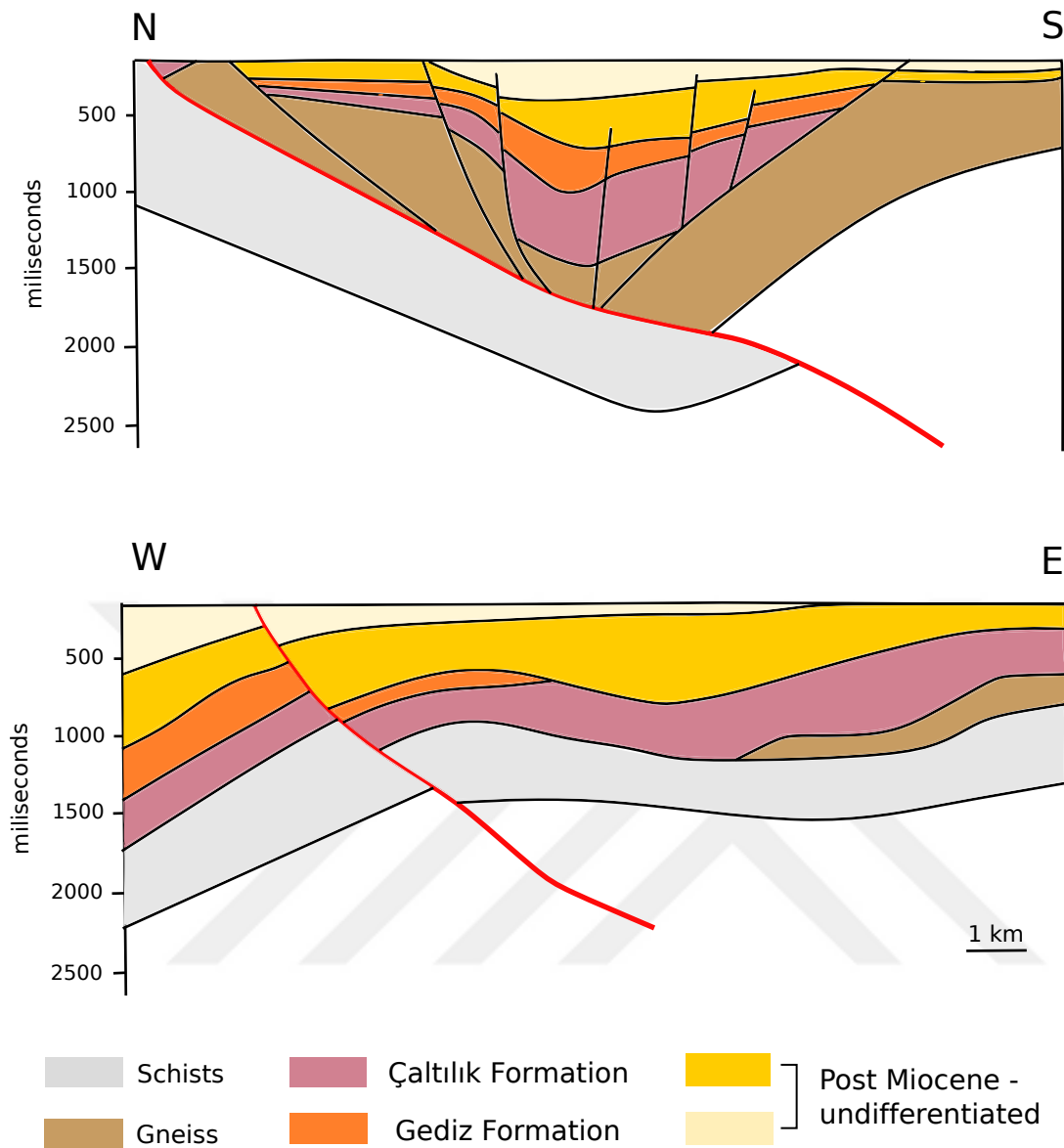


Figure 2.4: Seismic reflection studies for the Büyük Menderes detachment fault. a) N-S trending, seismic profile in association with the sequence stratigraphic unit, b) E-W trending, seismic profile in association with the sequence stratigraphic units. The red lines represent the main graben bounding fault (Simply modified from Çifçi, Pamukçu, Çoruh, Çopur, & Sözbilir (2011)).

The fault pattern of the graben perpendicular to its trend furthermore, it is complicated by the high-angle normal faults and the low-angle detachment fault. The dip of the detachment fault coincides well with the upper low-angle segment of the main graben bounding fault, emphasize the flat lying geometry. The lower segments is possibly original, the upper segments has possibly rotated to a low-angle. Structural data and fission track thermochronology studies (Gessner et al., 2001) also demonstrate that detachment in western Anatolia is produced by rotation.

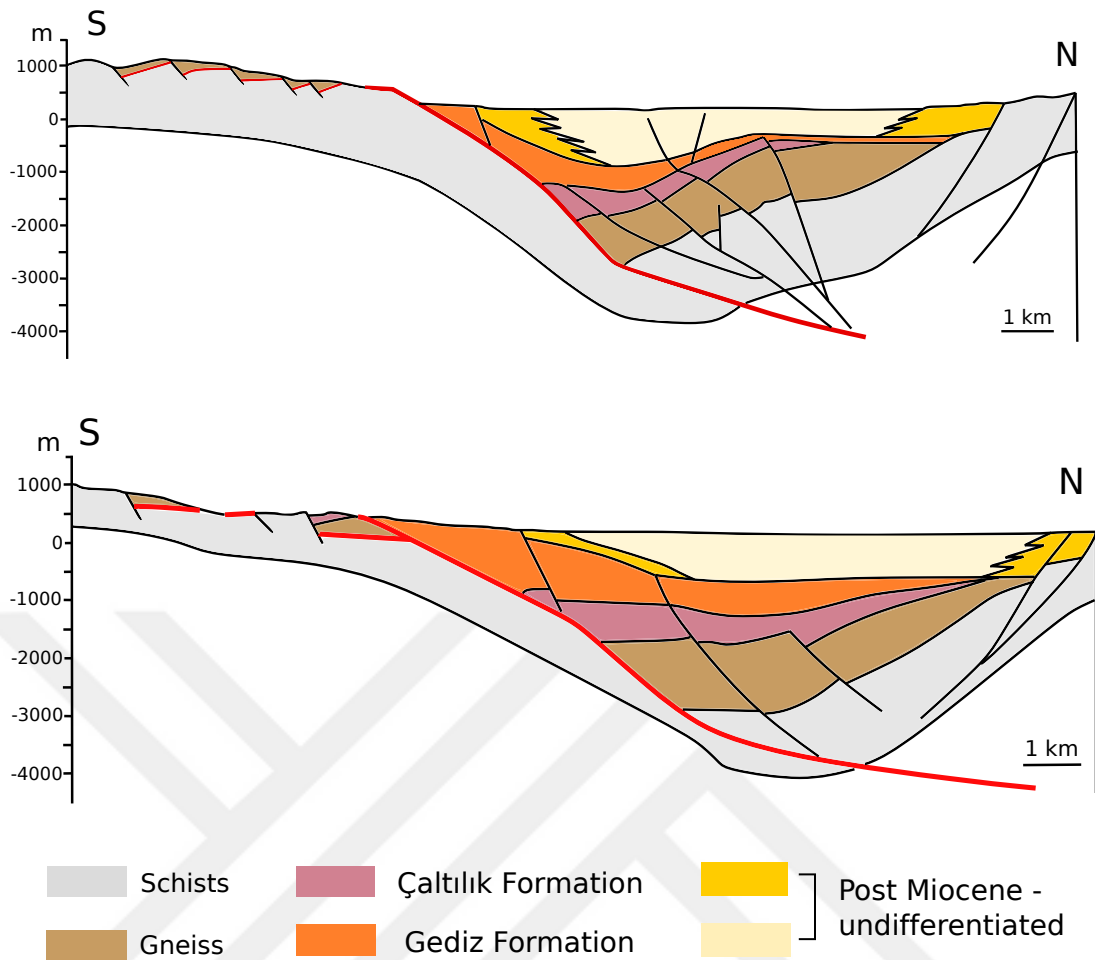


Figure 2.5: The interpreted seismic profiles were depth converted to link with the surface geology. Transverse geological cross-sections showing the geometry of the Gediz Graben. Both of the seismic profiles are trending with N-S direction. The red lines represent the main graben bounding fault (Simply modified from Çiftçi & Bozkurt (2010)).

Seismic studies show that; the detachment fault has 3 different segments on the surface. The oldest segment rotated around the horizontal axis and it almost has a flat pattern. The consideration of the fault migration towards the basin axis, the next fault is about 30° dip angle. The youngest is the boundary of the quaternary basin, which is active at present day and it has 60° dip angle. The faults where in the hanging wall are controlled with the detachment fault. Consequently, the detachment is formed at initially 60° angle at the surface furthermore, it loses its activity when it is rotated around horizontal axis under the effect of extension forces. It is crossed by the younger segment of the detachment fault and when this segment is rotated, it turns into a low-angle position. This segment is also losing its activity and is crossed to the basin towards younger segment of the detachment fault.

It is proposed that the Moho depth at western Anatolia changes by a two-stage extension. An Oligocene to Early-Miocene proposed gravitational collapse would have thinned the thickened crust to a homogeneous thickness of 25 km in a Basin and Range type extension of a hot and weak crust. And then, from the Early-Miocene, the extrusion of Anatolia would have amplified the extension to Moho depth smaller than 24 km, while the retreat of the Hellenic subduction slab.

Karabulut et al. (2013) suggests that crust-mantle boundary of the western Anatolia is not flat (undulation pattern) at regional scale. Moho depth ~25-30 km beneath the Menderes Massif depending on more than 2600 receiver functions. Broadcast asthenospheric flow patterns or intrusions of magmas into the crust and later modification of the crust are general features of the area.

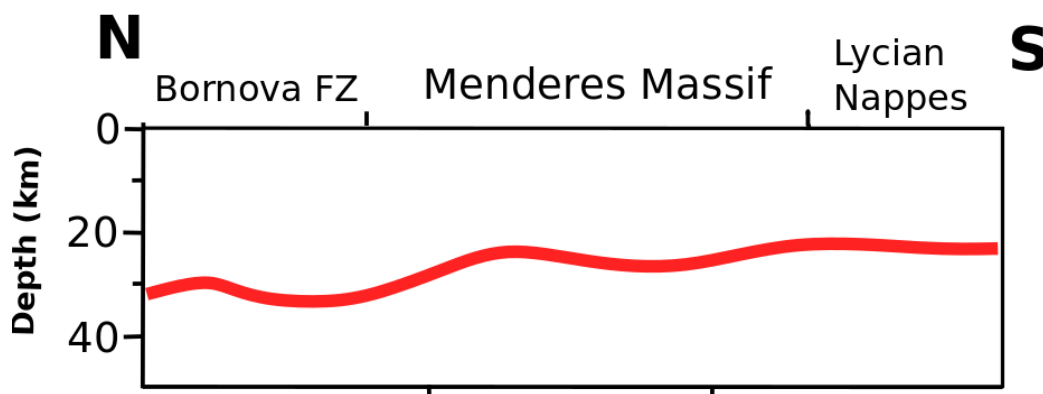


Figure 2.6: The red line shows the Moho depth that observed with the receiver function studies in the Bornova Flish Zone, Menderes Massif and the Lycian Nappes. Moho depth is 25-30 km beneath the Menderes Massif and its undulating structure seem (Karabulut et al., 2013).

2.3. Thermochronological Studies

Gessner et al. (2001) proposing that a large east-trending syncline within the Alpine nappe stack in the central part of the orogenic belt. Supposing continuous regional Alpine foliation and late Miocene cooling history across the western Anatolia, the syncline can be formed to an initial orientation. Back rotation of the syncline limbs present that the detachments rotated from high-angle to low-angle with an initial dip of $\sim 60^\circ$ for the Gediz and $\sim 40^\circ$ for the Büyük Menderes detachment.

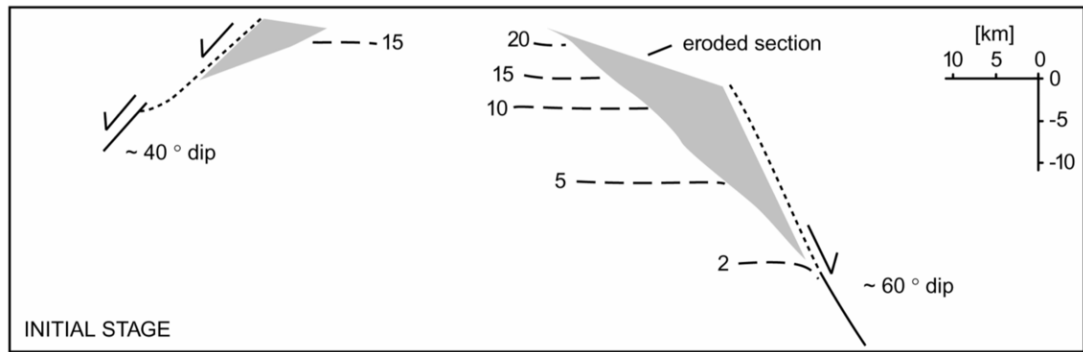


Figure 2.7: Fission-track data for the western Anatolia. Numbers with the dashed lines are the cooling ages (Gessner et al., 2001).

Another thermochronological study from Nilus et al., (2019), proposed that the low-angle normal faults contributed to the exhumation of the footwall. Thermokinematic modelling study of cooling ages from the footwall of the Büyük Menderes Detachment yielded exhumation rate of 0.5 km Ma^{-1} furthermore, high-angle normal faulting along the present Büyük Menderes graben commenced in the Quaternary ($\sim 3 \text{ Ma}$). It is indicated that the cooling ages of the footwall rocks is approximately 10-15 My and the hanging wall units is approximately 20-22 My (Fig. 2.8).

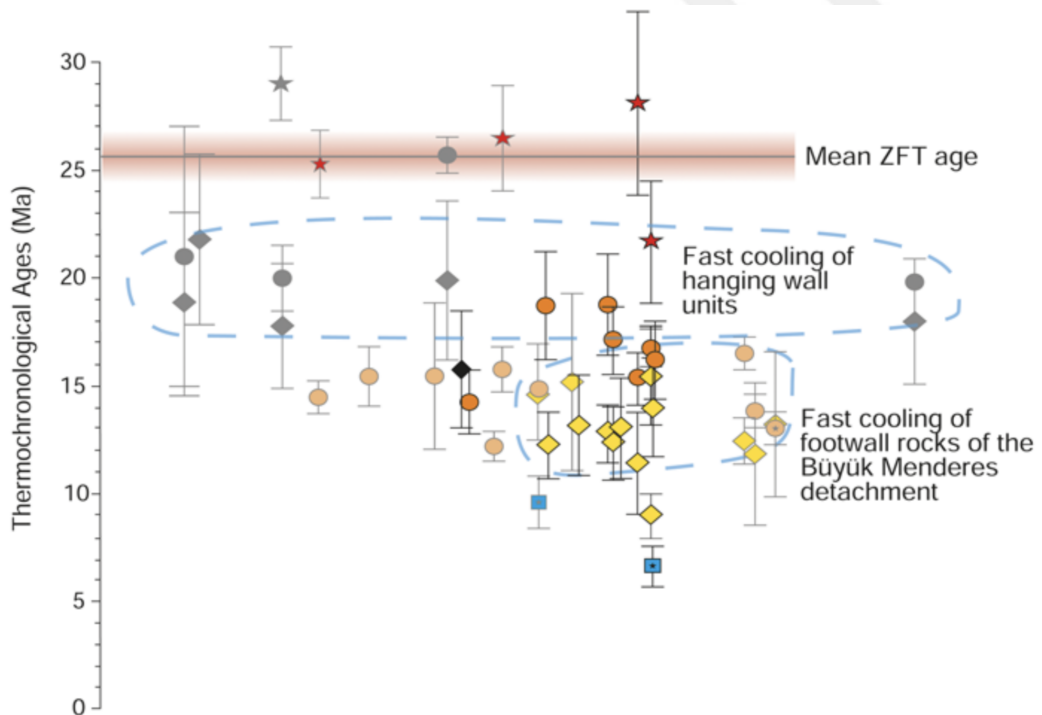


Figure 2.8 : Thermochronological results from Nilus et al., (2019) and show that the cooling ages of the rocks.

2.4. Objective of the Study

The mechanism of the evolution of detachment faults is still controversial and there are suggested theories about this problem. The main problem is the initial angle of the detachment faults. Also, the activity of these faults is not well-known problem and it is contradictive question. Here, we investigate the evolution of the normal fault systems on lithospheric scale using thermomechanical forward models. The aim of this study is to provide an approximation to the evolution of the detachment faults with the appropriate scale, time intervals and parameters.

Specifically, we focused on to test this main problem about the detachment faults for western Anatolia;

- We plan to invent the most suitable model to the current known of detachment faults in Western Anatolia. In doing so, we will test the proposed the rolling-hinge mechanism. We purpose to make an approach to the accuracy of these theory (Buck, 1988; Gessner et al., 2001; Seyitoğlu & Scott, 1996).
- The effect of the extension rate and the strain softening of the upper crust is known that huge impact on the fault development. We planned to test the effect of these parameters with preparing models sets that varying these parameters.

Overall, this research will provide new insight into development of the low-angle normal faults. The study can take advantage of geological, geophysical and thermomechanical information on the recent crustal deformation and lithospheric evolution by focusing on the western Anatolia region. As a result, we intend to focus the development of the detachment faults. Also, we can investigate that how the core complexes in Menderes Massif surfaced.

3. METHODOLOGY

3.1. Explanation of the Numerical Model

ASPECT (short for Advanced Solver for Problems in Earth's ConvecTion) that is an arbitrary Eulerian-Lagrangian finite element code for modeling the convection problems in the Earth's mantle with a Newtonian rheology will be used for the numerical modeling part of this work (Heister, Dannberg, Gassm oller, & Bangerth, 2017; Kronbichler, Heister, & Bangerth, 2012). This numerical code is useful for observing the development of the faults.

Governing equations of conservation of momentum (Eq. 3.1), mass (Eq. 3.2), and energy (Eq. 3.3) are;

$$-\nabla \cdot (2\mu_{\text{eff}} \dot{\epsilon}(\mathbf{u})) + \nabla P = \rho \mathbf{g}, \quad (3.1)$$

$$\nabla \cdot \mathbf{u} = 0, \quad (3.2)$$

$$\frac{\partial T}{\partial t} + \mathbf{u} \cdot \nabla T - \nabla \cdot (\kappa + \nu_h(T)) \nabla T = 0. \quad (3.3)$$

In equations 3.1, 3.2 and 3.3, μ_{eff} , $\dot{\epsilon}$, \mathbf{u} , P , ρ , \mathbf{g} represent the effective viscosity (Pa.s), is the strain rate (1/s), the velocity vector (m s^{-1}), total pressure (Pa), density (kg m^{-3}) and gravity vector (kg m^{-2}). Likewise, T , t , κ , ν_h are variables symbolizing temperature (273  K), time (s), thermal diffusivity ($\text{m}^2 \text{s}^{-1}$) and artificial diffusivity ($\text{m}^2 \text{s}^{-1}$). Artificial diffusivity ν_h is used to prevent oscillations due to the advection of the temperature field.

$$\frac{\partial c_i}{\partial t} + \mathbf{u} \cdot \nabla c_i - \nabla \cdot (\nu_h(c_i)) \nabla c_i = 0. \quad (3.4)$$

Material parameters are represented by compositional fields which are advected with the flow. c_i represents the compositional field in the equation 3.4 that introduces an additional advection equation to the system of equations 3.1 and 3.3.

Density, ρ , in the models is function of temperature and composition: $\rho = \rho_0(1 - \alpha(T - T_0))$; where α is the coefficient of thermal expansion (K^{-1}), T_0 is the reference temperature (K°), and ρ_0 is the reference density ($kg\ m^{-3}$) that depends on material.

There are three main rheologies implemented that can be combined into more complex ones:

1. bulk diffusion creep
2. power-law dislocation creep
3. plastic yielding.

Rheologies 1 and 2 can be formulated with one equation:

$$\mu_{\text{eff}} = \frac{1}{2} K \left(\frac{d}{b}\right)^{\frac{m}{n}} \left(\frac{1}{A}\right)^{\frac{1}{n}} \dot{\epsilon}_e^{\frac{(1-n)}{n}} \exp\left(\frac{Q+PV}{nRT}\right). \quad (3.5)$$

In equation 3.5, μ_{eff} , K , d , b , m , n represents effective viscosity (Pa s), shear modulus (80 GPa), grain size (0.01 m), burgers vector length (0.5×10^{-9} m), grain size exponent that is dimensionless and stress component. Similarly, A is the pre-extensional factor ($Pa^{-n}\ s^{-1}$), $\dot{\epsilon}_e$ is the effective deviatoric strain rate (s^{-1}), Q is the activation energy ($J\ mol^{-1}$), P is the total pressure (Pa), V is the activation volume ($m^3\ mol^{-1}$), R is the ideal gas constant ($8.314\ J\ K^{-1}\ mol^{-1}$), and T is the absolute temperature (K). With this formula, in case of diffusion creep, $n = 1$ and $m > 0$, while for dislocation creep $n > 1$, and $m = 0$.

Drucker-Prager criterion is implemented for rheology 3 which is:

$$\sigma^y = C \cos(\emptyset) + \sin(\emptyset)P. \quad (3.6)$$

In equation 3.6, σ^y is the yield value, C is the cohesion (20 GPa), P is the pressure (Pa) and \emptyset is an internal angle of friction. For 2-D models this equation is equal the Mohr-Coulomb criterion (Eq. 3.7).

$$\tau = \sigma \tan(\emptyset) + c \quad (3.7)$$

Where the τ is a shear stress (Pa), σ is a normal stress (Pa), \emptyset is an internal angle of friction (degree) and c is the cohesion (20 GPa).

3.2. Model Setup

The initial condition of our model is designed to reproduce the first-order lithospheric structure at the onset of Western Anatolia extension approximately 20 million years

Table 3.1 : Model parameters for the different layers of the reference model. Other parameters are assumed to be constant. But their sensitivity on the results may be tested in future experiments.

Reference Model	Upper Crust	Lower Crust	Mantle Lithosphere	Asthenosphere
ρ Density	2700 kg m ⁻³	2850 kg m ⁻³	3280 kg m ⁻³	3300 kg m ⁻³
κ Thermal diffusivity	7.71x10 ⁻⁷ m ² s ⁻¹	7.31x10 ⁻⁷ m ² s ⁻¹	8.38x10 ⁻⁷ m ² s ⁻¹	8.33x10 ⁻⁷ m ² s ⁻¹
α Thermal expansivity	2.7x10 ⁻⁵ K ⁻¹	2.7x10 ⁻⁵ K ⁻¹	2.7x10 ⁻⁵ K ⁻¹	2.7x10 ⁻⁵ K ⁻¹
m Grain size exponent for diffusion creep	2	3	0	0
B_{dl} Prefactor for dislocation creep	8.57x10 ⁻²⁸ Pa ⁻ⁿ s ⁻¹	7.13x10 ⁻¹⁸ Pa ⁻ⁿ s ⁻¹	6.52x10 ⁻¹⁶ Pa ⁻ⁿ s ⁻¹	6.52x10 ⁻¹⁶ Pa ⁻ⁿ s ⁻¹
n_{dl} Stress exponent for dislocation creep	4	3	3.5	3.5
Q_{dl} Activation energies for dislocation creep	223x10 ³ J mol ⁻¹	345x10 ³ J mol ⁻¹	530x10 ³ J mol ⁻¹	530x10 ³ J mol ⁻¹
V_{dl} Activation volumes for dislocation creep	0	38x10 ⁻⁶ m ³ mol ⁻¹	18x10 ⁻⁶ m ³ mol ⁻¹	18x10 ⁻⁶ m ³ mol ⁻¹
B_{df} Prefactor for diffusion creep	5.97x10 ⁻¹⁹ Pa ⁻ⁿ s ⁻¹	2.99x10 ⁻²⁵ Pa ⁻ⁿ s ⁻¹	2.25x10 ⁻²⁵ Pa ⁻ⁿ s ⁻¹	2.25x10 ⁻²⁵ Pa ⁻ⁿ s ⁻¹
n_{df} Stress exponent for diffusion creep	1	1	1	1
Q_{df} Activation energies for diffusion creep	223x10 ³ J mol ⁻¹	159x10 ³ J mol ⁻¹	375x10 ³ J mol ⁻¹	375x10 ³ J mol ⁻¹
V_{df} Activation volumes for diffusion creep	0	38x10 ⁻⁶ m ³ mol ⁻¹	6x10 ⁻⁶ m ³ mol ⁻¹	6x10 ⁻⁶ m ³ mol ⁻¹

ago and consists of an upper crust (25 km thick) with wet quartzite rheology (Gleason & Tullis, 1995), a lower crust (25 km thick) with wet anorthite rheology (Rybacki & Dresen, 2000), and a mantle lithosphere (30 km thick) with dry olivine rheology (Hirth & Kohlstedt, 2003).

Numerical experiments are conducted within the solution box 500 km width and 165 km height. The model setup is exposed to an equal amount of the extension rates from the left and right boundary of the model, moreover the total of these rates is the full-rate of the extension. The model is imposed to extension along the entire vertical planes further, the outflow of the material during the extension is supported with the inflow of the asthenosphere from the bottom.

It suggested that a collision before the extension at the region approximately 40 Ma. (Dilek, 2006), therefore a thick crust (50 km) is imposed in the model setup. Also, it is proposed that the mantle lithosphere is thinner than expected depending on the magmatism at region in Neogene time (Şengör, Görür, & Şaroğlu, 1985). It is thought that this magmatism started with the thinning of the mantle lithosphere under gravitational forces and the asthenosphere flow into the examined edges (Göğüş, Pysklywec, Şengör, & Gün, 2017). Because of this reason thin (30 km) mantle lithosphere conducted to the model setup (Figure 3.1).

Development of the faults depending on the extension rate and the friction weakening factor of the upper crust are studied so, any weak zone or pre-existing faults are not conducted at the model setup. We conduct two model suits where we investigate the impact of key parameters within a plausible range: (1) we vary the extension velocities imposed on the margins of the model boundary from $V_{ext} = 1-4$ cm/year full rate. (2) We vary the friction strain weakening factor $\varepsilon = 0.1$ to 0.5 for the upper crust with an internal friction angle of $\phi = 20^\circ$. These two parameters have been varied to be compatible values.

In the model set, we started with our model setup and the temperature at lithosphere-asthenosphere boundary (LAB) was set as 1300°C . The densities (ρ) of the upper crust, lower crust, mantle lithosphere and asthenosphere were set as 2700 kg/m^3 , 2850 kg/m^3 , 3280 kg/m^3 and 3300 kg/m^3 .

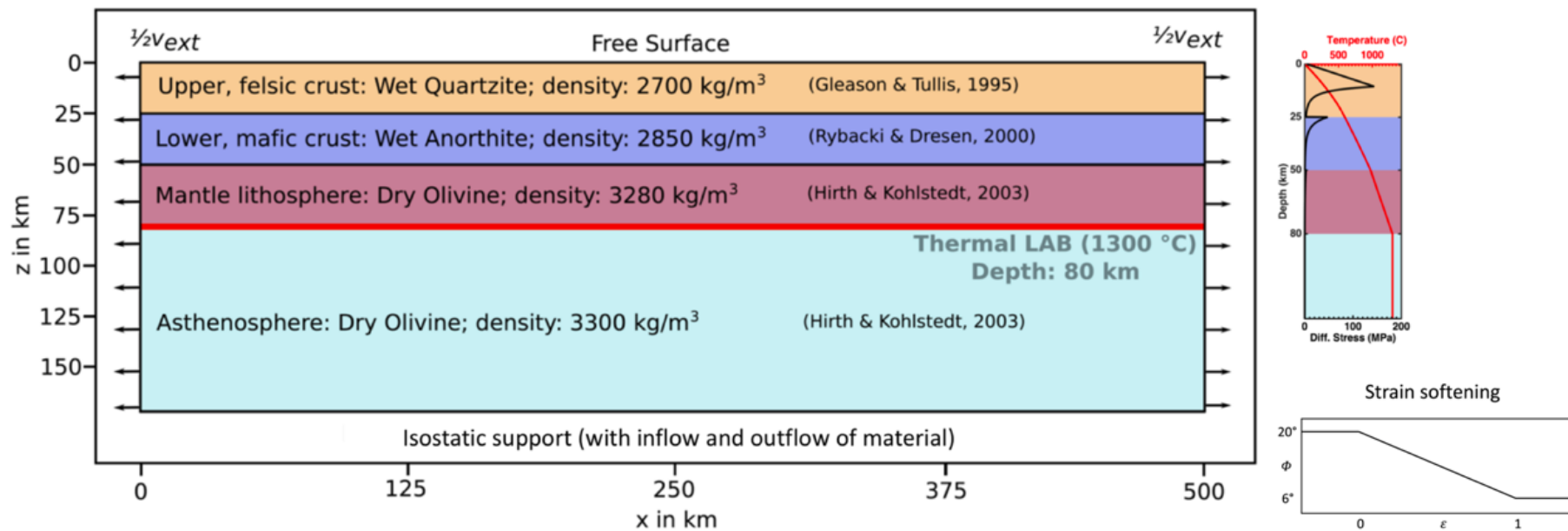


Figure 3.1 : Model setup for the extensional tectonics in the western Anatolia and the strength and the strain softening profiles. Orange: Upper crust, Purple: Lower crust, Red: Lithospheric mantle, Blue: Asthenosphere.

3.3. Measurement of Fault Angles

Measurement of fault angles is based on a basic mathematical principle. The ratio of the differences of the x and y values of the two points whose coordinates are known is equal to the tangent of the remaining angle (Eq. 3.7).

$$\frac{(x_2 - x_1)}{(y_2 - y_1)} = \tan(\theta) \quad (3.7)$$

Initially the angles of the faults are the same because the fault has only one direction. Due to rolling-hinge mechanism, it can be seen that the faults have a lower angle towards near the surface and a higher angle in the direction of deeper part. The angles of the faults were measured from upper part of the fault in order to be compatible with the angles measured in the geological field studies. When measuring these angles, a horizontal axis was drawn from the point where the fault was curved and the angle between them (θ) was measured.

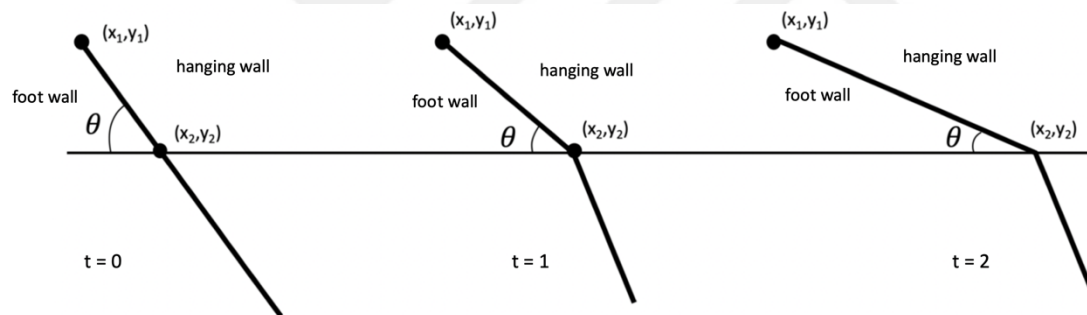


Figure 3.2: Cartoon shows the measurement of the angles of the faults at different time step due to rolling-hinge mechanism.

4. MODEL RESULTS

4.1. Reference Model

A number of models were constructed using the mentioned parameters above. After a series of experiment, the model with the extension rate of 2 cm/year, the friction strain weakening factor of the upper crust of 0.3 and the internal angle of friction 20° was selected as a reference model.

The strain rates are shown in the figures and the places where these values are focused and high represent faults. The lower crust is the purple areas, hence the lower bound of this region, represents the Moho. Due to the rheology of the lower crust, faults did not descend to this area and were concentrated in the upper crust. In order to follow the development of the faults easier, 45 kilometers depth were used in the figures.

In the reference model, deformation occurs to be localized due to extension and all faults have initially 50° - 55° angles after 2 My. model started. After 6 My. conjugate fault system is seen in the model domain and it is remarkable that deformation is concentrated in certain places. When the model continues, a strain localization at the opposing symmetrical faults (facing against each other) in the center of the model domain and on the hanging-wall of these main breakaway faults, new higher-angle normal faults develop after 14 million years. It has been suggested that these new high-angle normal faults correspond to the main antithetic fault observed in seismic studies. The mechanism of rotation of the breakaway fault and the small-displaced block on its hanging wall consequences mainly from differential isostatic adjustment due to thinning/exhumation of the crust. The Moho exhumation that depends on the isostatic rebound, the angles of the opposing symmetrical faults decrease moreover, Moho shows undulate pattern because of the same reason. Also, the depth of the Moho is approximately 25-30 km under the symmetric faults. Here, it can be said that the undulation pattern of Moho is rheologically because of the viscos behavior. In approximately, 20 million years after the model begins, such symmetrical low-angle fault system develops (10° - 14°) at shallow depths (e.g., 10 km below the surface).

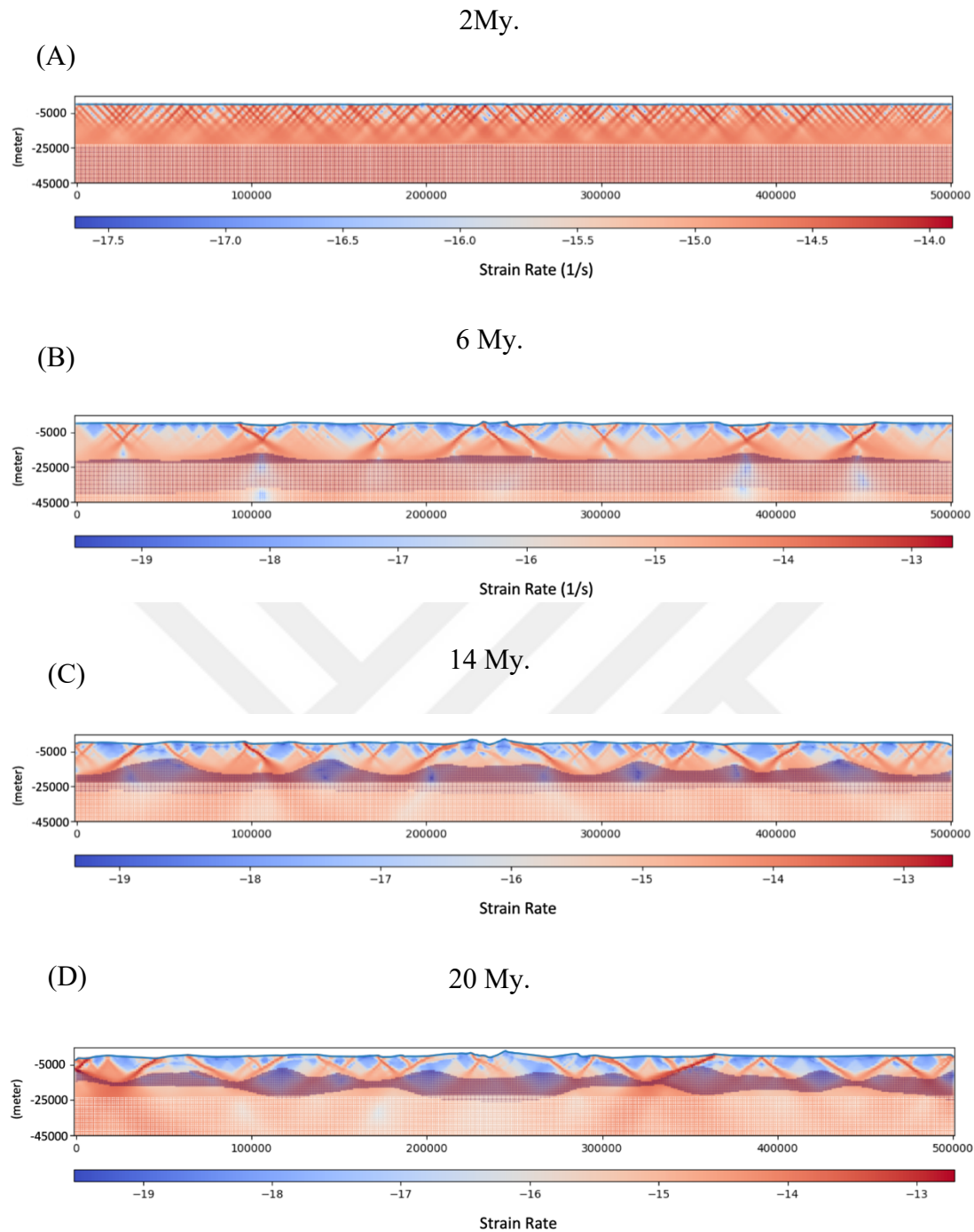


Figure 4.1: Fault development of model with extension 1 cm/yr. (A) after 2 My., (B) after 6 My., (C) after 14 My., (D) after 20 My. The top of the model represents the upper crust, purple areas represent the lower crust. Regions where the strain rate is red colored deformation is high.

Again, there are also new high-angle normal faults at the hanging-wall of these shallow dipping faults. In addition, the exhumed massif has a dome shaped structure and the distance to one another is comparable to those of Western Anatolia.

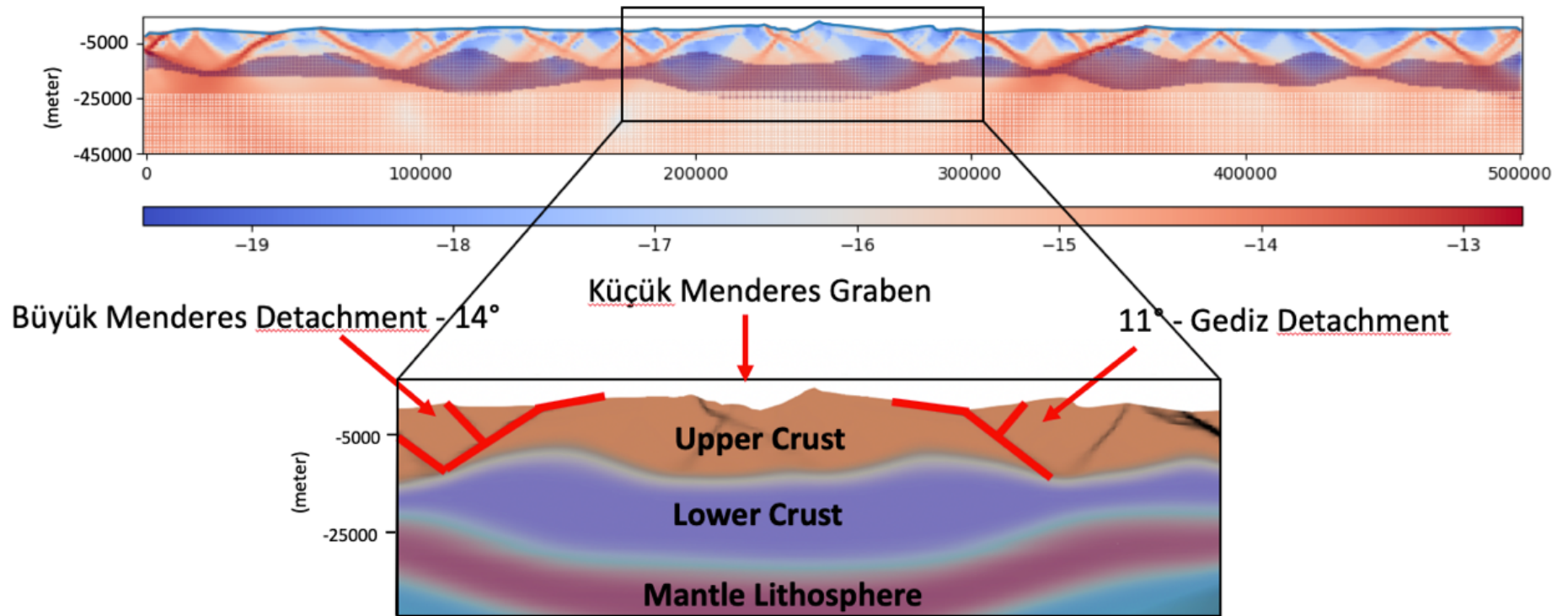


Figure 4.2 : 22 My. after model started and the last time step of the reference model.

Reference model supports the two rolling-hinge detachment system separated by elongated metamorphic domes with fold axes perpendicular to the direction of extension. If we named the two opposing symmetrical faults as Gediz and Büyük Menderes detachments at the last time step of the model, the area between these faults refers to Küçük Menderes graben (Figure 4.2). If we consider that lower crust starts at 25 kilometers deep in the model setup and is at approximately 15 kilometers deep in the last model step, it can be suggested that it rises about 10 kilometers.

4.1.1. Extension rate effect

Extension rate plays an important role on the development of the faults so, it is varied to see the effect of the parameter. These parameters were changed between 1 and 4 cm/yr. in accordance with data obtained from GPS studies. Friction strain weakening factors for the upper crust and the internal angle of the frictions are the equal with the reference model thus, just the effect of the extension rate is seen in this model set.

At the models with different extension rate, it can be said that this parameter has an important role in fault development. When the extension rate was set 1cm/yr., as it can be seen from Fig. 4.3 that the angle of the faults does not decrease to less than 20 degrees. The extension rate does not allow the fault angles to decline sufficiently, but also the distance between the faults are not adequate with the study area. It can be said that the deformation is localized later stage due to the decreasing in extension rate. The faults have not a symmetrical pattern furthermore, the new high-angle normal faults have not developed in conjunction with them. It is seen that the undulation pattern of the Moho is less than the reference model and depth of the Moho is about 35 km. Also, the dome shape structure is not observed in this model.

If the extension rate is increased to 3 cm/yr., as in the reference model, it can be observed that the deformation is localized in certain places and two symmetrical faults are observed. It can be said that there are new high-angle normal faults in conjunction with these symmetric faults. The undulation pattern of the Moho due to isostatic adjustment and the dome structure are also agreeable with the western Anatolia but, after 20 million year the model start, the crustal break up is seen in the model (Fig. 4.4). It is known that there is no such break up in the region, so this model is not suitable for Western Anatolia.

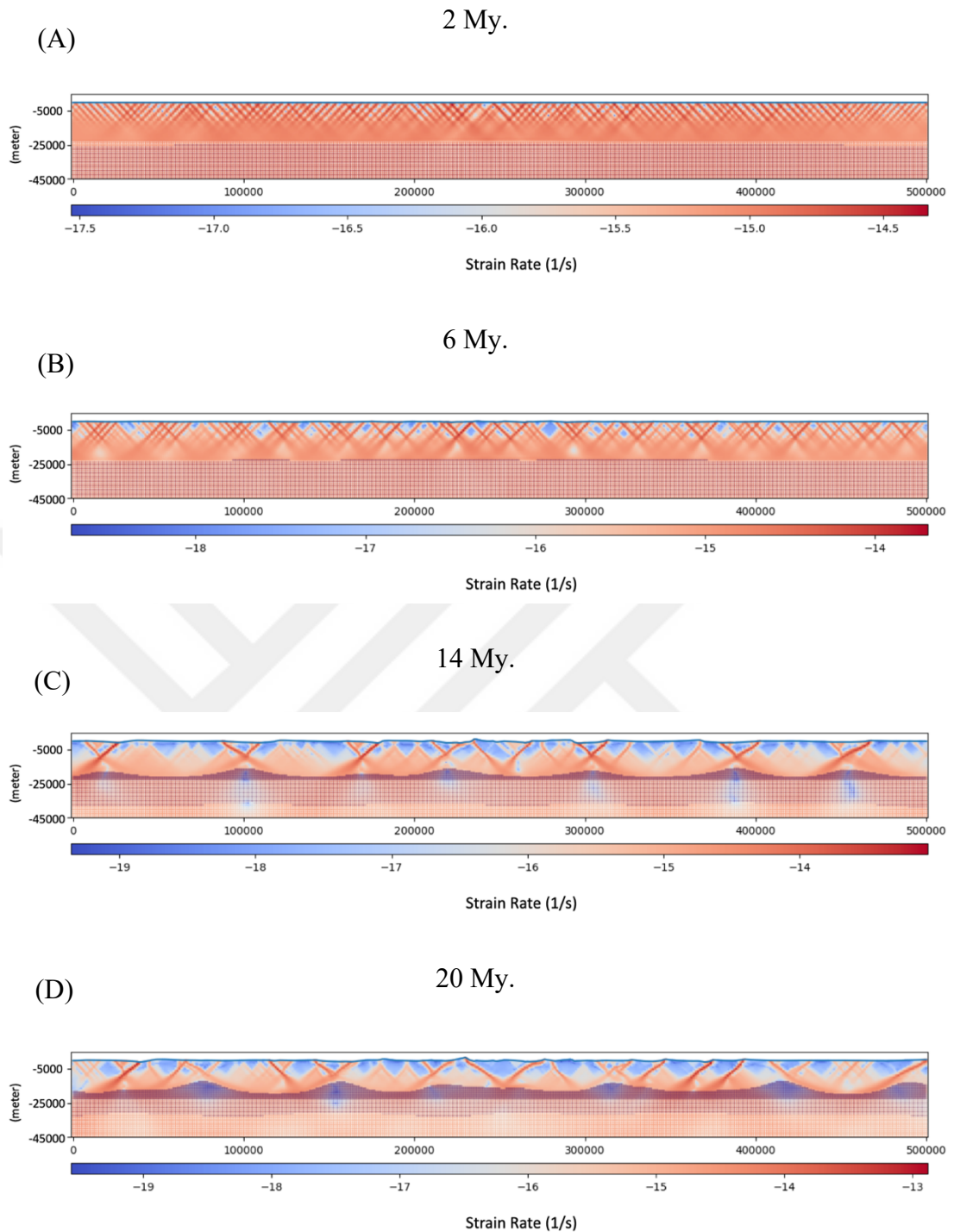


Figure 4.3: Fault development of model with extension 1 cm/yr. (A) after 2 My., (B) after 6 My., (C) after 14 My., (D) after 20 My. The top of the model represents the upper crust, purple areas represent the lower crust. Regions where the strain rate is red colored deformation is high.

Increasing the extension rate to 4 cm/yr. it is clearly seen that the strain localization and the response to isostatic adjustment is happening at earlier stage and therefore, the angles of the faults decrease much earlier than the reference model. In the center of

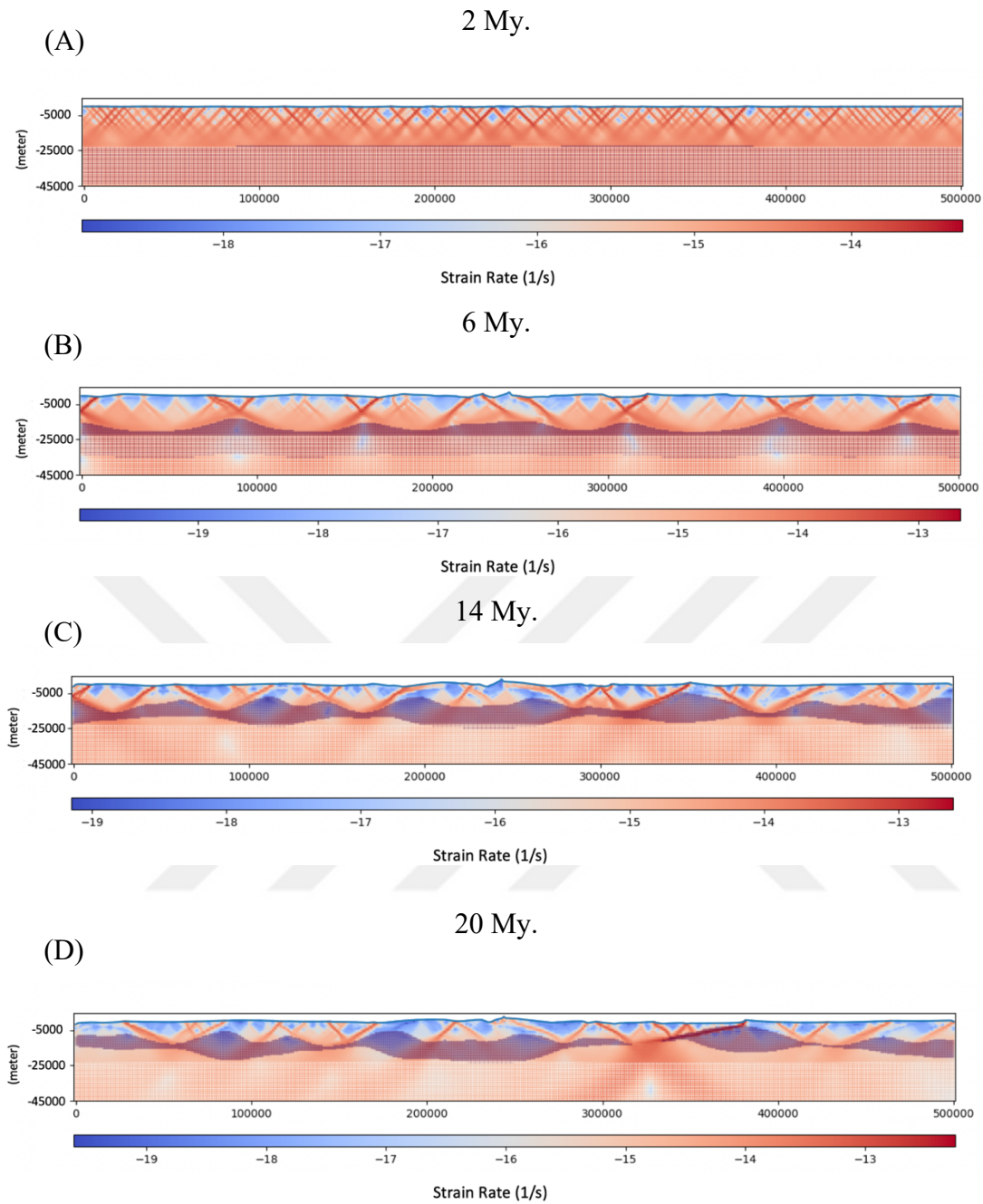


Figure 4.4: Fault development of model with extension 3 cm/yr. (A) after 2 My., (B) after 6 My., (C) after 14 My., (D) after 20 My. The top of the model represents the upper crust, purple areas represent the lower crust. Regions where the strain rate is red colored deformation is high.

this model, it can be said that faults have a symmetrical pattern and dome shape structure at 6 My. In addition, it can be seen that the new high-angle normal faults have developed and Moho shows an undulation pattern and its depth is approximately 25 km. However, this model provides a break up as well (Fig. 4.5) moreover, this break up just happening after 14 million years model start. Also, the symmetrical fault

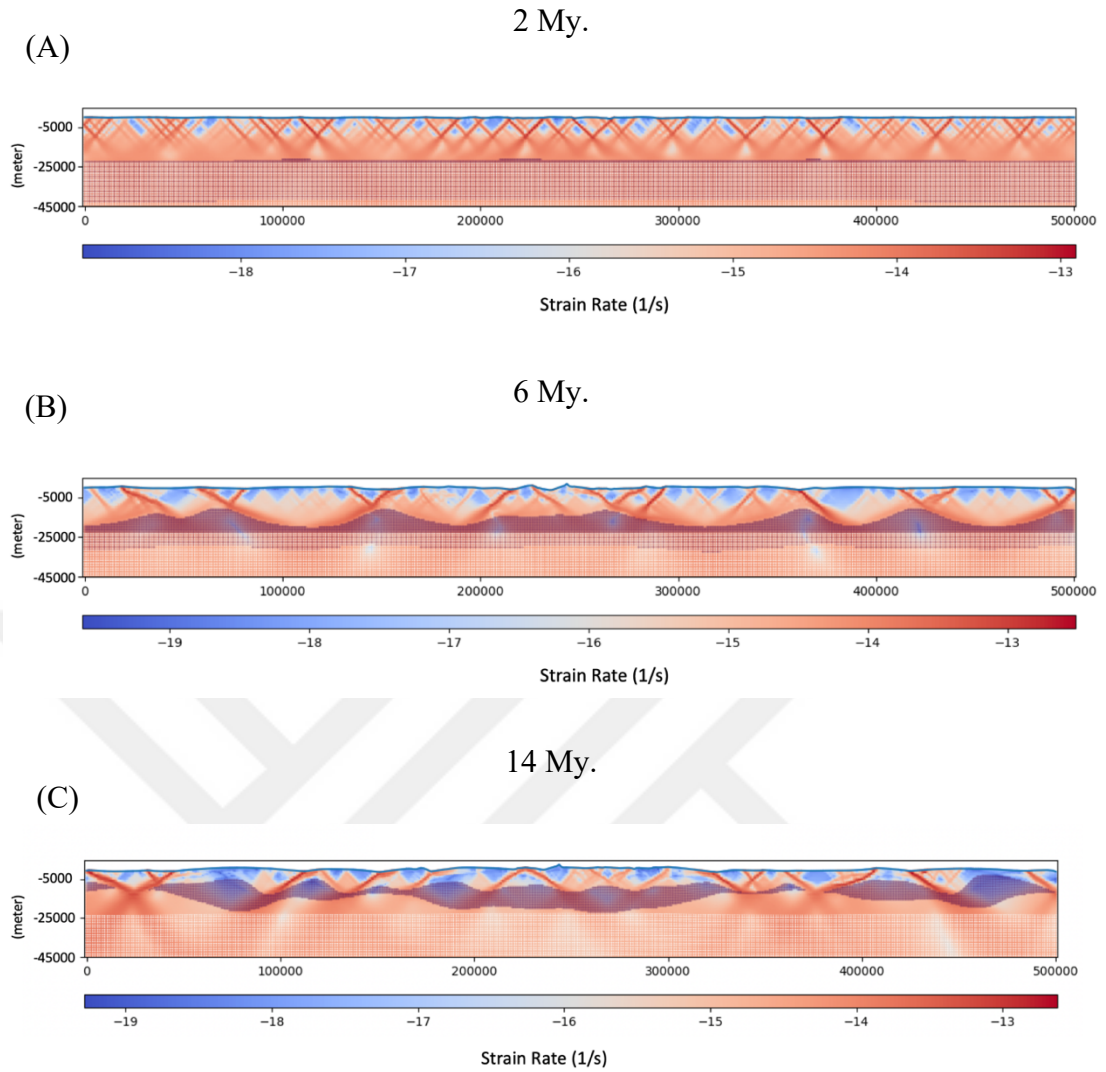
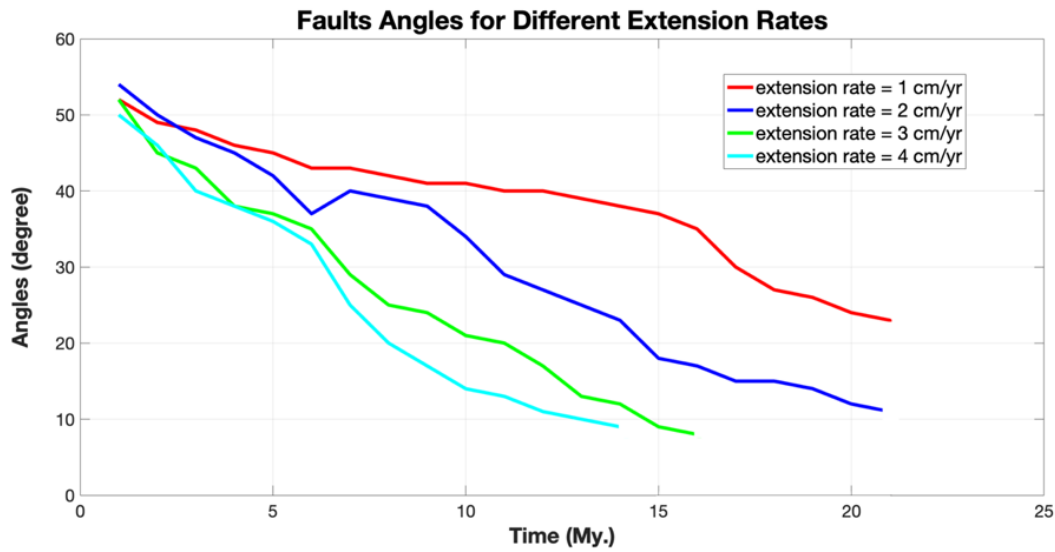


Figure 4.5: Fault development of model with extension 4 cm/yr. (A) after 2 My., (B) after 6 My., (C) after 14 My.. The top of the model represents the upper crust, purple areas represent the lower crust. Regions where the strain rate is red colored deformation is high.

pattern is missing at 14 My., so it can be said that this model is not agreeable for western Anatolia. Table 4.1 shows the shows the changing the angles of the faults depending on time. It is clearly seen that when the extension rate increases, the fault angles decrease more quickly. In models other than the model where the opening speed is 1 cm/yr., the angles of the faults are around 10 degrees. However, the continental break up at 3 and 4 cm/yr, angles make these models incompatible. Because in the light of studies, this is not the case in Western Anatolia.

Table 4.1: Fault angles for different extension rates depending on time. Strain weakening factor and the internal angle of friction remained the same value.



4.1.2. Friction strain weakening factor of the upper crust effect

Another parameter that varied in this study is the friction strain weakening factor of the upper crust and these parameters were changed between 0.1 and 0.5. The studies have argued that the strain weakening factor has a significant role in the symmetry of the faults (Huisman & Beaumont, 2002), so this parameter has been tested in this work. Extension rates and the internal angle of the frictions are the equal with the reference model thus, just the effect of the weakening factor is seen in this model set.

When the friction strain weakening factor of the upper crust is set 0.1, the upper crust is weaker than the reference model therefore, it is observed that the strain is localized much earlier and the model responds more quickly to the isostatic rebound. After 6 My., it can be said that there are two faults that develop symmetrically in the center of the model, but because of that respond, the angles of these faults have decreased earlier than the reference model. It can be proposed that Moho has an undulation pattern and its depth is approximately 25 km in 14 My. after the experiment begin (Fig. 4.6).

If friction strain weakening factor of the upper crust is decreased to 0.2, the model is not really different from the reference model and it is observed that all faults initiate with 50°-55° angles. 6 million years after the beginning of the experiment, it is seen that the deformation is localized and two opposing symmetrical faults develop. As the

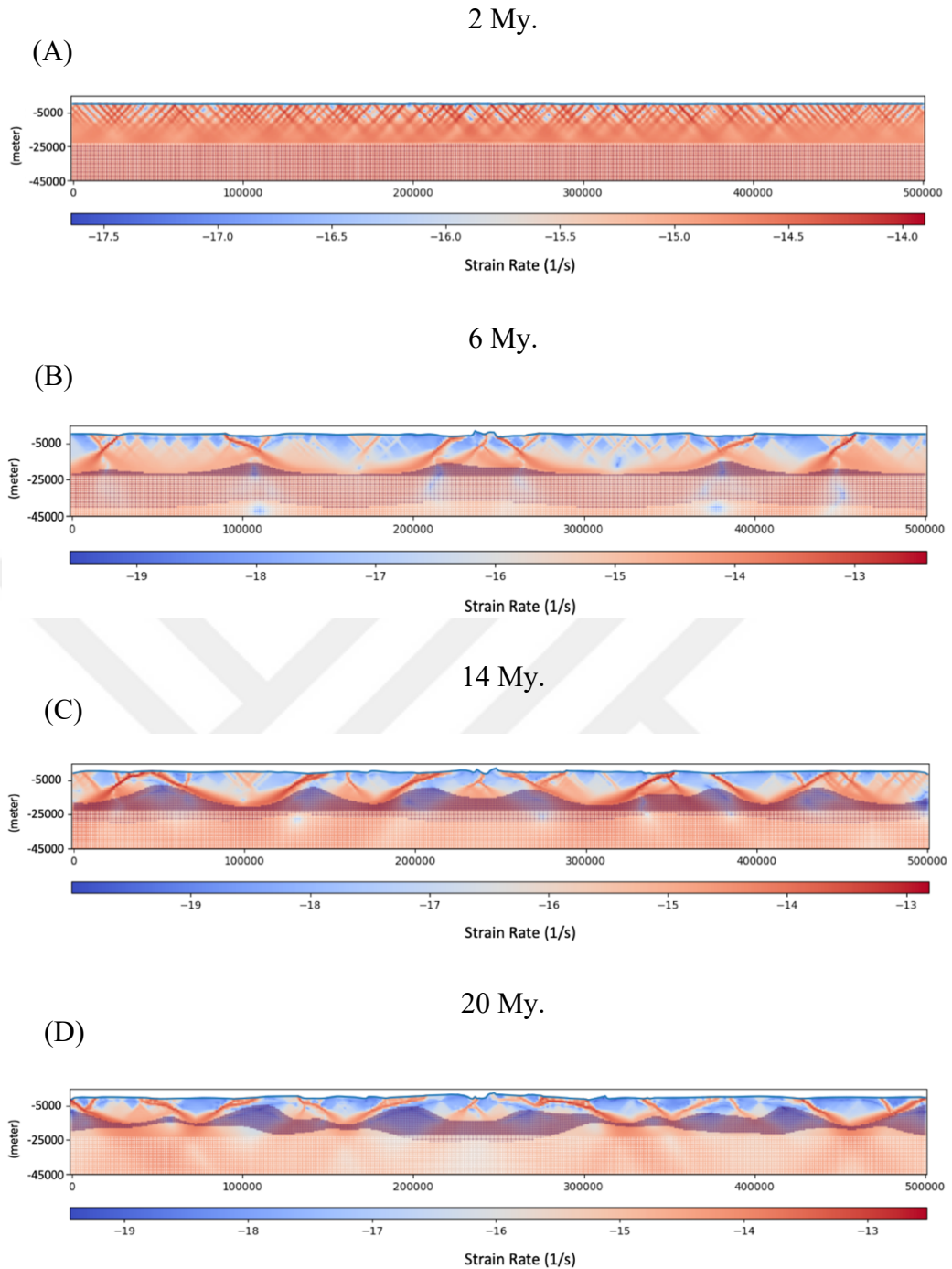


Figure 4.6: Fault development of model with the friction weakening factor of the upper crust is 0.1. (A) after 2 My., (B) after 6 My., (C) after 14 My., (D) after 20 My. The top of the model represents the upper crust, purple areas represent the lower crust. Regions where the strain rate is red colored deformation is high.

model continues, the angles of the faults decrease and the undulation pattern of Moho is observed as a response of the isostatic rebound due to the extension. It can be said that the Moho depth is between 25 and 30 km under that these symmetric faults and the center of the model has a dome shape structure (Fig. 4.7).

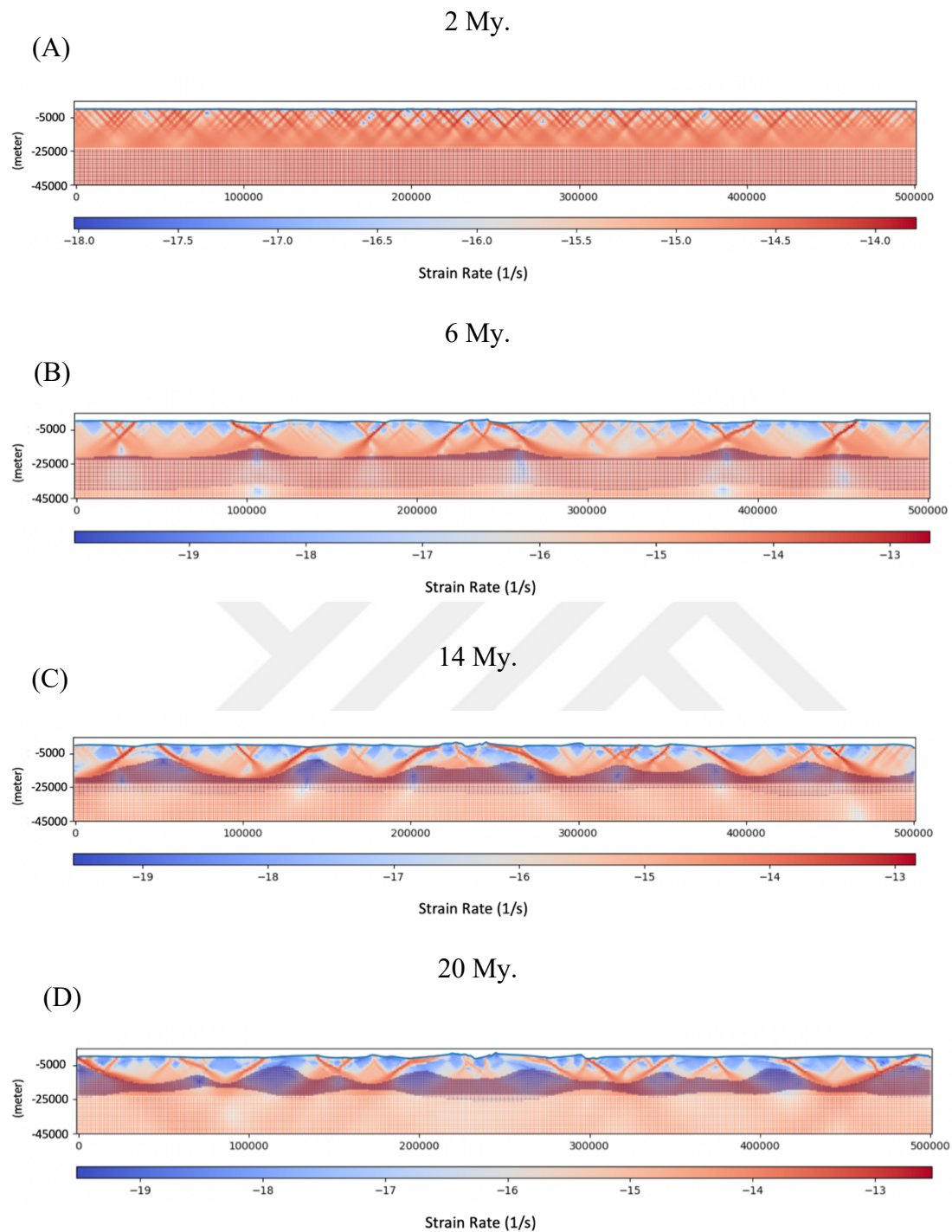


Figure 4.7: Fault development of model with the friction weakening factor of the upper crust is 0.2. (A) after 2 My., (B) after 6 My., (C) after 14 My., (D) after 20 My. The top of the model represents the upper crust, purple areas represent the lower crust. Regions where the strain rate is red colored deformation is high.

When the strain weakening factor of the upper crust is increased to 0.4, the upper crust is stronger than the reference model. After 6 My. it is seen that strain localized and

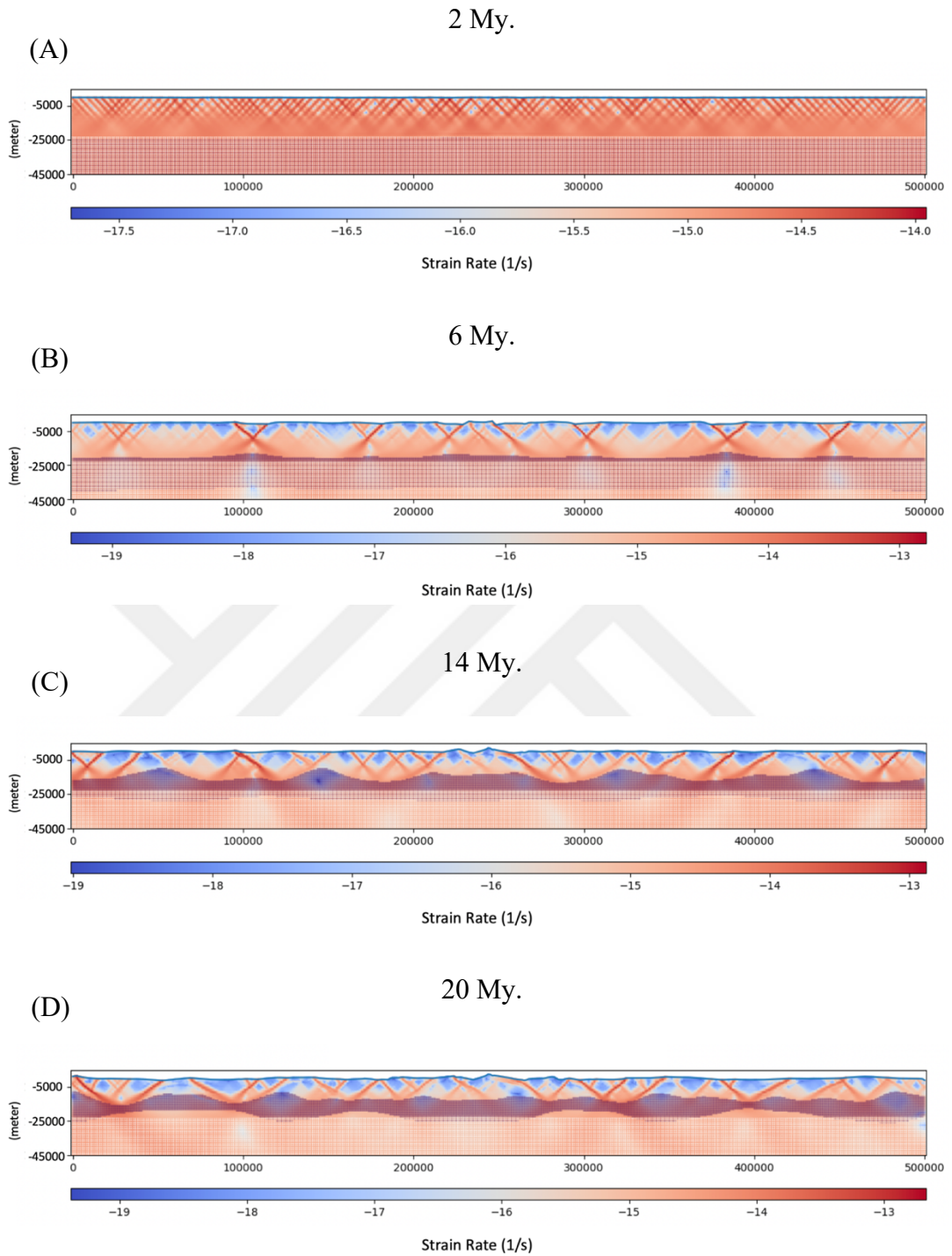


Figure 4.8: Fault development of model with the friction weakening factor of the upper crust is 0.4. (A) after 2 My., (B) after 6 My., (C) after 14 My., (D) after 20 My. The top of the model represents the upper crust, purple areas represent the lower crust. Regions where the strain rate is red colored deformation is high.

symmetric faults are developed in center of the model. However, due to the increase of the strength of the upper crust, the angles of the faults gradually decrease over time and a large number of faults are observed compared to the previous models. It can be

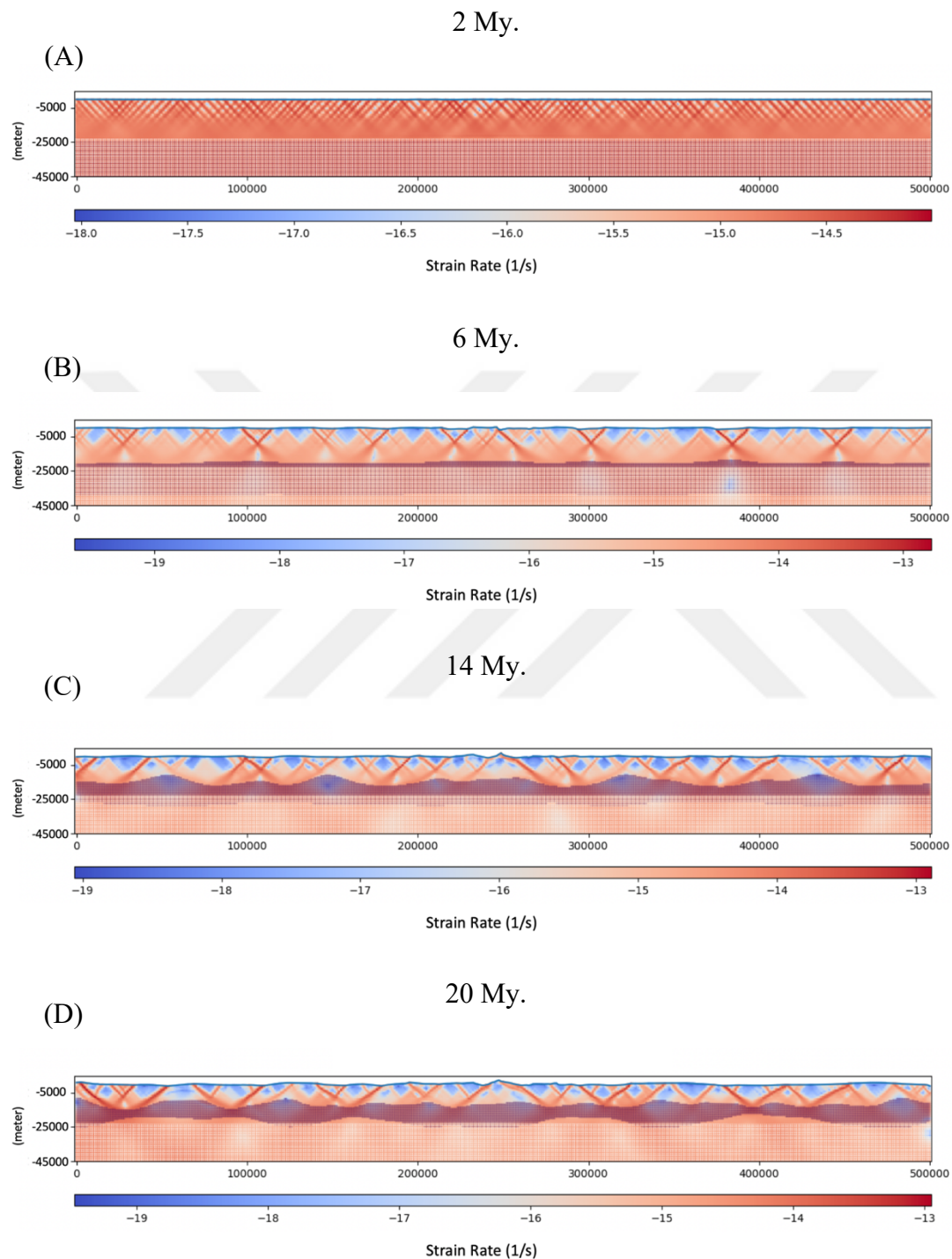


Figure 4.9: Fault development of model with the friction weakening factor of the upper crust is 0.5. (A) after 2 My., (B) after 6 My., (C) after 14 My., (D) after 20 My. The top of the model represents the upper crust, purple areas represent the lower crust. Regions where the strain rate is red colored deformation is high.

said that Moho does not have a undulation pattern, has a nearly flatten shape furthermore, its depth is about 25 kilometers deep. Because of this shape of the Moho, dome shape structure is not observed. (Fig. 4.8.).

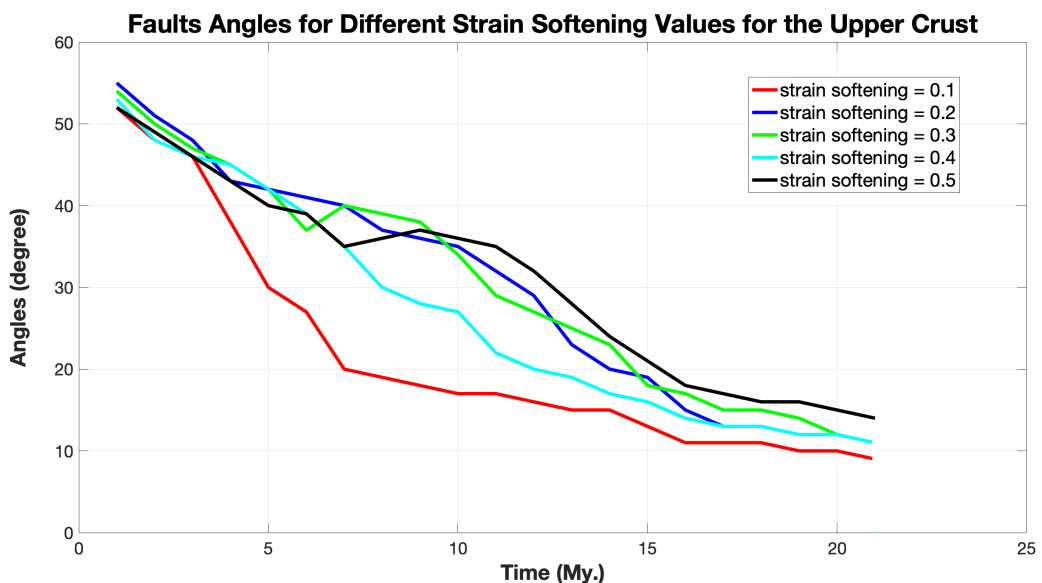
If the strain weakening factor of the upper crust is increased to 0.5, depending on the strength of the upper crust, the deformation localized later than the reference model.

In the center of the model, two symmetrical faults are seen but the angles of these faults are higher for western Anatolia. It can be said that Moho has a flat structure as in the previous model and its depth is approximately 25 kilometers. (Fig. 4.9). With the increase of this parameter value, it has been observed that the upper crust becomes more strength and the angles of the faults decrease later than the reference model

(Table 4.2). In addition, it can be said that the number of faults caused by the increase in this parameter value increases. It is seen that Moho does not have an undulation pattern and so, the dome shape structure is not observed.

An important point in these experiments, so far these models suggest that strain weakening factor is not the major controlling factor for the symmetry of the faults. Although this parameter has been changed, it is seen that the faults are symmetrical in all models.

Table 4.2: Fault angles for different strain weakening factor for the upper crust values depending on time. Extension rates and the internal angle of friction remained the same value





5. MODEL RESULTS AGAINST OBSERVATIONS

Our model results show that normal faults initiate with a high-angle and as a response to isostatic rebound, they rotate to low-angle. The development of the faults are dependent on the extension rate and strain softening of the upper crust.

Figure 5.1a shows the reference extension experiment result at 22 My. The model results are compared with the seismic reflection studies for the Gediz and Büyük Menderes detachment faults (Çiftçi et al., 2011; Çiftçi & Bozkurt, 2010). Seismic studies show the fault pattern of the detachment faults and high-angle normal faults are in conjunction with them. Because of the model domain, just the detachment faults and the main antithetic faults are seen in the model results. The same patterns of the faults are observed between the observations and the model.

Figure 5.1b indicates that the large-scale receiver function studies performed across through the western Anatolia region, it was suggested that the Moho depth is approximately 25-30 km beneath the Menderes massif (Karabulut et al., 2013). Depending on the extension, the undulation pattern of the Moho is prominent in response to isostatic rebound. The identical undulation pattern of the Moho is observed in the reference model. Therefore, the depth of the Moho for the last time step (22 My) of the reference model is approximately 25-30 km. These are the good agreement with the proposed receiver function studies.

In Figure 5.2, the suggested initial faults for the Gediz and Büyük Menderes detachment faults with thermochronological fission-track study (Gessner et al., 2001). It is proposed that the detachment faults rotated from high-angle to low-angle moreover, the initial angles of the faults are computed as roughly 60° and 40°. The faults are initiate between 50°-55° angles in the reference model. So, these orientations of the faults are agreeable with the fission track studies.

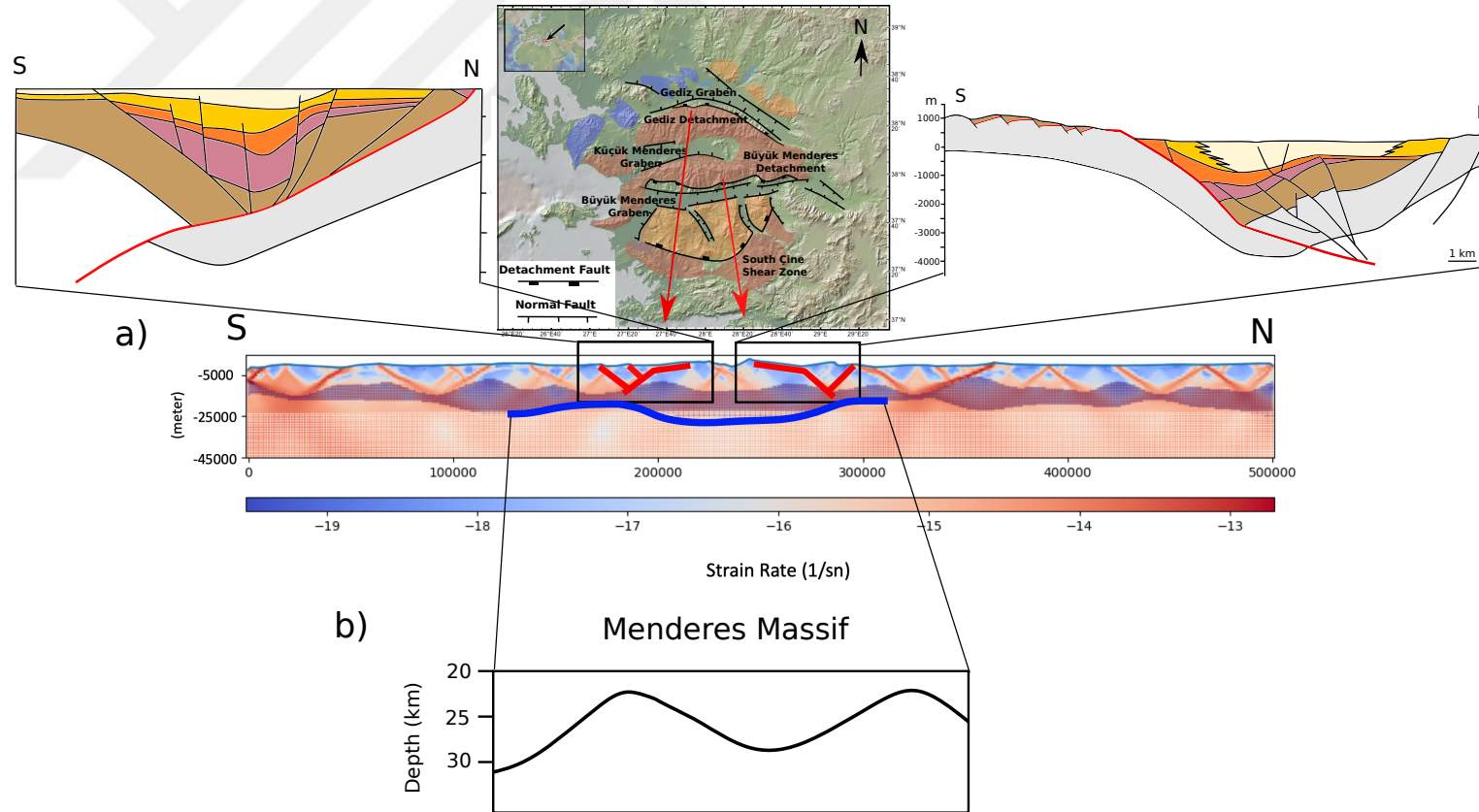


Figure 5.1 : (a) The reference model at $t = 22$ My and the observed seismic reflection profiles for the Gediz and Büyük Menderes detachment faults (Çifçi et al., 2011; Çiftçi & Bozkurt, 2010). (b) Observed Moho topography from receiver function studies (Karabulut et al., 2013)

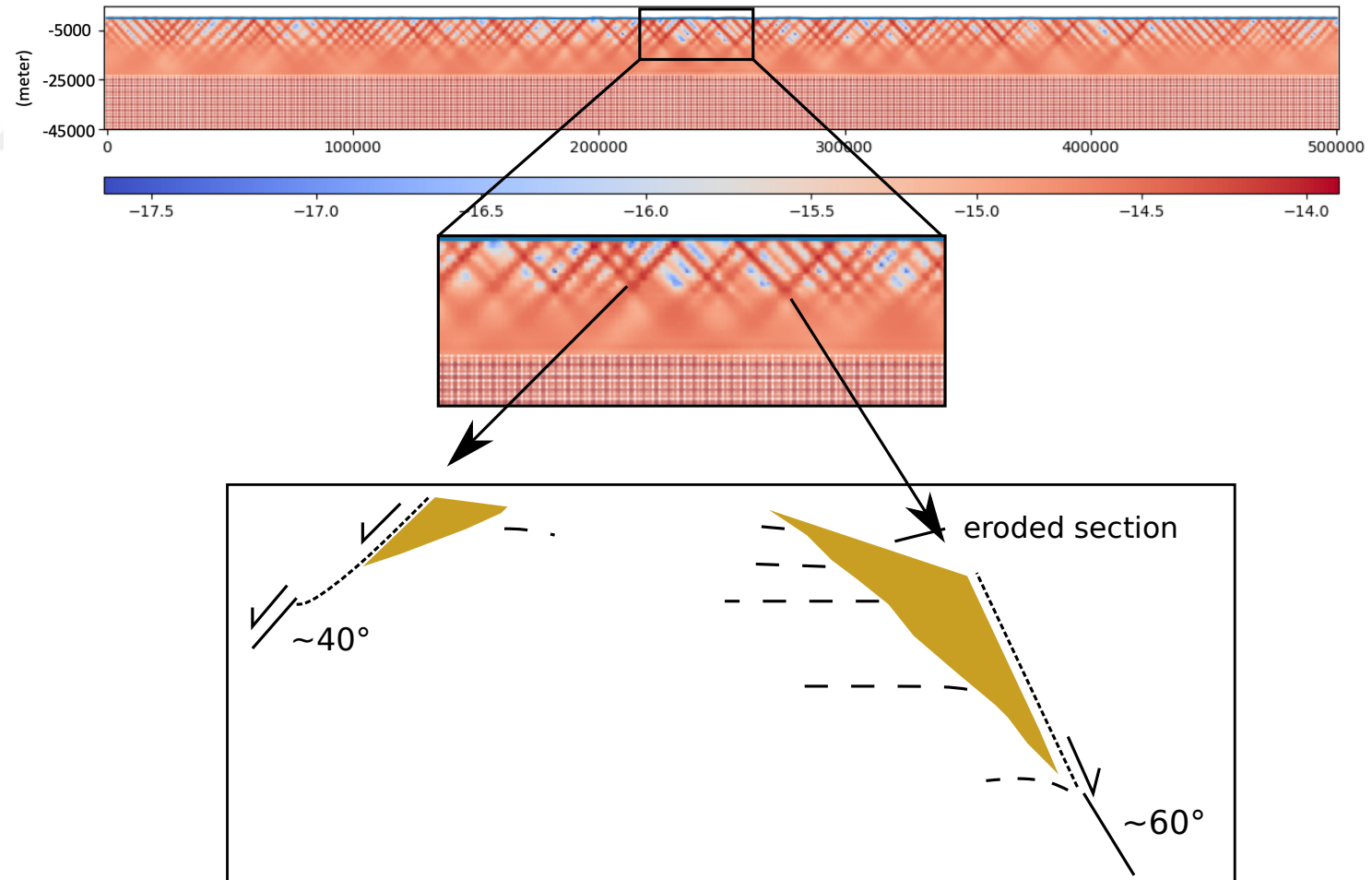


Figure 5.2 : The reference model at $t = 2$ My and fission-track study for the initial fault angles (Gessner et al., 2001)

Our experimental work suggests that two major low angle detachment faults (dipping in 10° - 15°) in the central part of western Anatolia are formed by rolling hinge mechanism where the faults angles rotate from initially 55° . This is in good agreement with the field observations. Strain softening control the time dependent evolution of the faults, but so far, our results suggest that this is not the major controlling factor for the symmetry- asymmetry of the shearing. Future models will help us to the understand better why the opposite dipping normal faults and the related shear sense in the Aegean-western Anatolia back arc system are common features



REFERENCES

- Abbott, L. D., Silver, E. A., Anderson, R. S., Smith, R., Ingle, J. C., Kling, S. A., ... Sliter, W.** (1997). Measurement of tectonic surface uplift rate in a young collisional mountain belt. *Nature*.
- Akçay, M., Özkan, H. M., Moon, C. J., & Scott, B. C.** (1996). Secondary dispersion from gold deposits in West Turkey. *Journal of Geochemical Exploration*.
- Aldanmaz, E., Pearce, J. A., Thirlwall, M. F., & Mitchell, J. G.** (2000). Petrogenetic evolution of late Cenozoic, post-collision volcanism in western Anatolia, Turkey. *Journal of Volcanology and Geothermal Research*, 102, 67–95.
- Anderson, E. M.** (1905). The Dynamics of Faulting. *Transactions of the Edinburgh Geological Society*, 8(3), 387–402.
- Armstrong, R. L.** (1972). Low-Angle (Denudation) Faults, Hinterland of the Sevier Orogenic Belt, Eastern Nevada and Western Utah. *Geological Society of America Bulletin*, 83, 1729–1754.
- Bartley, J. M., & Wernicke, B. P.** (1984). The Snake Range Décollement Interpreted as a Major Extensional Shear Zone. *Tectonics*, 3(6), 647–657.
- Bozkurt, E., & Park, L. R. G.** (1994). Southern Menderes Massif: an incipient metamorphic core complex in western Anatolia, Turkey. *Journal of the Geological Society*, 151(2), 213–216.
- Bozkurt, E., Winchester, J. A., & Park, R. G.** (1995). Geochemistry and tectonic significance of augen gneisses from the southern Menderes Massif (West Turkey). *Geological Magazine*, 132(3), 287–301.
- Bozkurt, Erdin, & Sözbilir, H.** (2004). Tectonic evolution of the Gediz Graben: Field evidence for an episodic, two-stage extension in western Turkey. *Geological Magazine*, 141(1), 63–79.
- Buck, W. R.** (1988). Flexural Rotation of Normal Faults. *Tectonics*, 7(5), 959–973.
- Carpenter, B. M., Saffer, D. M., & Marone, C.** (2015). Frictional properties of the active San Andreas Fault at SAFOD: Implications for fault strength and slip behavior. *Journal of Geophysical Research: Solid Earth*, 120(7), 5273–5289.
- Çifçi, G., Pamukçu, O., Çoruh, C., Çopur, S., & Sözbilir, H.** (2010). Shallow and Deep Structure of a Supradetachment Basin Based on Geological, Conventional Deep Seismic Reflection Sections and Gravity Data in the Buyuk Menderes Graben, Western Anatolia. *Surveys in Geophysics*. <https://doi.org/10.1007/s10712-010-9109-8>
- Çifçi, G., Pamukçu, O., Çoruh, C., Çopur, S., & Sözbilir, H.** (2011). Shallow and Deep Structure of a Supradetachment Basin Based on Geological, Conventional Deep Seismic Reflection Sections and Gravity Data in the Buyuk Menderes Graben, Western Anatolia. *Surveys in Geophysics*, 32(3), 271–290. <https://doi.org/10.1007/s10712-010-9109-8>
- Çiftçi, N. B., & Bozkurt, E.** (2010). Structural evolution of the Gediz Graben, SW

- Turkey: Temporal and spatial variation of the graben basin. *Basin Research*, 22(6), 846–873. <https://doi.org/10.1111/j.1365-2117.2009.00438.x>
- Cohen, H. A., Dart, C. J., Akyüz, H. S., & Barka, A.** (1995). Syn-rift sedimentation and structural development of the Gediz and Büyük Menderes graben, western Turkey. *Journal of the Geological Society*, 152, 629–638. <https://doi.org/10.1144/gsjgs.152.4.0629>
- Dewey, J. F., & Sengor, A. M. C.** (1979). Aegean And Surrounding Regions - Complex Multi-Plate And Continuum Tectonics In A Convergent Zone. *Geological Society of America Bulletin*, 90(1), 84–92.
- Dilek, Y.** (2006). Collision tectonics of the Mediterranean region : *Geological Society of America Special Paper*. [https://doi.org/10.1130/2006.2409\(01\)](https://doi.org/10.1130/2006.2409(01)).
- Emre, T., & Sözbilir, H.** (1997). Field evidence for metamorphic core complex, detachment faulting and accommodation faults in the Gediz and Büyük Menderes grabens, western Anatolia. *Turkish Journal of Earth Sciences*.
- Gessner, K., Ring, U., Johnson, C., Hetzel, R., Passchier, C. W., & Güngör, T.** (2001). An active bivergent rolling-hinge detachment system: Central Menderes metamorphic core complex in western Turkey. *Geological Society of America*, 29(7), 611–614.
- Gleason, G. C., & Tullis, J.** (1995). A flow law for dislocation creep of quartz aggregates determined with the molten salt cell. *Tectonophysics*, 247(1–4), 1–23.
- Göğüş, O. H., Pysklywec, R. N., Şengör, A. M. C., & Gün, E.** (2017). Drip tectonics and the enigmatic uplift of the Central Anatolian Plateau. *Nature Communications*, 8(1). <https://doi.org/10.1038/s41467-017-01611-3>
- Heister, T., Dannberg, J., Gassmöller, R., & Bangerth, W.** (2017). High accuracy mantle convection simulation through modern numerical methods - II: Realistic models and problems. *Geophysical Journal International*. <https://doi.org/10.1093/gji/ggx195>
- Hetzel, R., & Reischmann, T.** (1996). Intrusion age of Pan-African augen gneisses in the southern Menderes Massif and the age of cooling after Alpine ductile extensional deformation. *Geological Magazine*, 133(5), 565–572.
- Hetzel, R., Romer, R. L., Candan, O., & Passchier, C. W.** (1998). Geology of the Bozdag area, central Menderes massif, SW Turkey: Pan-African basement and Alpine deformation. *Geologische Rundschau*, 87(3), 394–406.
- Hirth, G., & Kohlstedt, D.** (2003). Rheology of the Upper Mantle and the Mantle Wedge: A View from the Experimentalists. *Inside the Subduction Factory Geophysical Monograph*, 138, 83–105.
- Hreinsdóttir, S., & Bennett, R. A.** (2009). Active aseismic creep on the Alto Tiberina low-angle normal fault, Italy. *Geology*, 37(8), 683–686.
- Huismans, R. S., & Beaumont, C.** (2002). Asymmetric lithospheric extension: The role of frictional plastic strain softening inferred from numerical experiments. *Geology*, 30, 211–214.
- Jackson, J. A.** (2008). Active normal faulting and crustal extension. *Geological Society, London, Special Publications*.
- Jackson, J. A., & White, N. J.** (1989). Normal faulting in the upper continental crust: observations from regions of active extension. *Journal of Structural*

- Geology*, 11, 15–36. [https://doi.org/10.1016/0191-8141\(89\)90033-3](https://doi.org/10.1016/0191-8141(89)90033-3)
- Jolivet, L., & Brun, J. P.** (2010). Cenozoic geodynamic evolution of the Aegean. *International Journal of Earth Sciences*.
- Karabulut, H., Paul, A., Ergün, T. A., Hatzfeld, D., Childs, D. M., & Aktar, M.** (2013). Long-wavelength undulations of the seismic Moho beneath the strongly stretched Western Anatolia. *Geophysical Journal International*, 194, 450–464.
- Koçyiğit, A., Yusufoglu, H., & Bozkurt, E.** (1999). Evidence from the Gediz graben for episodic two-stage extension in western Turkey. *Journal of the Geological Society*.
- Kronbichler, M., Heister, T., & Bangerth, W.** (2012). High accuracy mantle convection simulation through modern numerical methods. *Geophysical Journal International*. <https://doi.org/10.1111/j.1365-246X.2012.05609.x>
- Lavier, L. L., Buck, W. R., & Poliakov, A. N. B.** (1999). Self-consistent rolling-hinge model for the evolution of large-offset low-angle normal faults. *Geology*, 27(12), 1127–1130. [https://doi.org/10.1130/0091-7613\(1999\)027<1127:SCRHMF>2.3.CO;2](https://doi.org/10.1130/0091-7613(1999)027<1127:SCRHMF>2.3.CO;2)
- Lips, A. L. W., Cassard, D., Sözbilir, H., Yilmaz, H., & Wijbrans, J. R.** (2001). Multistage exhumation of the Menderes Massif, Western Anatolia (Turkey). *International Journal of Earth Sciences*, 89(4), 781–792.
- Longwell, C. R.** (1945). Low-Angle Normal Faults in the Basin-and-Range Province. *Transactions, American Geophysical Union*, 26, 107–118.
- Miller, E. L., Gans, P. B., & Garing, J.** (1983). The Snake Range décollement: An exhumed mid-Tertiary ductile–brittle transition. *Tectonics*, 2(3), 239–263.
- Nilius, N.-P., Glotzbach, C., Wölfler, A., Hampel, A., Dunkl, I., Akal, C., ... Hetzel, R.** (2019). Exhumation history of the Aydın range and the role of the Büyük Menderes detachment system during bivertent extension of the central Menderes Massif, western Turkey. *Journal of the Geological Society*. <https://doi.org/10.1144/jgs2018-162>
- Nocquet, J. M.** (2012). Present-day kinematics of the Mediterranean: A comprehensive overview of GPS results. *Tectonophysics*.
- Platt, J. P., Behr, W. M., & Cooper, F. J.** (2014). Metamorphic core complexes: windows into the mechanics and rheology of the crust. *Journal of the Geological Society*, 172(1), 9–27.
- Rigo, A., Lyon-Caen, H., Armijo, R., Deschamps, A., Hatzfeld, D., Makropoulos, K., ... Kassaras, I.** (1996). A microseismic study in the western part of the Gulf of Corinth (Greece): Implications for large-scale normal faulting mechanisms. *Geophysical Journal International*, 126(3), 663–688.
- Rybacki, E., & Dresen, G.** (2000). Dislocation and diffusion creep of synthetic anorthite aggregates. *Journal of Geophysical Research: Solid Earth*.
- Şengör, A. M. C., Görür, N., & Şaroğlu, F.** (1985). Strike-slip Faulting and Related Basin Formation in Zones of Tectonic Escape: Tukey as a Case Study. *The Society of Economic Paleontologists and Mineralogist*, 227–264.
- Seyitoğlu, G., & Scott, B. C.** (1996). The cause of N-S extensional tectonics in western Turkey: Tectonic escape vs back-arc spreading vs orogenic collapse. *Journal of Geodynamics*, 22, 145–153.
- Seyitoglu, G., Tekeli, O., Çemen, İ., Şen, Ş., & Işık, V.** (2002). The role of the

- flexural rotation/rolling hinge model in the tectonic evolution of the Alaşehir graben, western Turkey. *Geological Magazine*, 139(1), 15–26.
- Sözbilir, H., & Emre, T.** (1996). Menderes Masifi'nin neotektonik evriminde oluşan supradetachment havzalar ve rift havzaları (Supradetachment basin and rift develop during the neotectonic evolution of the Menderes Massif.). *49th Geological Congress of Turkey 49th*, 30–31.
- Townend, J.** (2006). What Do Faults Feel? Observational Constraints on the Stresses Acting On Seismogenic Faults. *American Geophysical Union, Geophysical Monograph*, 170, 313–327.
- Wernicke, B.** (1981). Low-angle normal faults in the Basin and Range Province: nappe tectonics in an extending orogen. *Nature*, 291, 645–648.
- Wernicke, B., & Axen, G. J.** (1988). On the Role of Isostasy in the Evolution of Normal Fault Systems. *Geology*, 16, 848–851.
- Yılmaz, Y., Genç, Ş. C., Gürer, F., Bozcu, M., Yılmaz, K., Karacik, Z., ... Elmas, A.** (2008). When Did the Western Anatolian Grabens Begin to Develop? *Geological Society, London, Special Publications*.



CURRICULUM VITAE



Name Surname : Ömer BODUR
Place and Date of Birth : Istanbul-Turkey / 23.08.1993
E-Mail : bodurom@itu.edu.tr

EDUCATION :

- **B.Sc.** : 2017, Istanbul Technical University, Faculty of Mines, Geophysical Engineering Department
- **M.Sc.** : 2019, Istanbul Technical University, Eurasia Institute of Earth Science, Geodynamics Programme

PROFESSIONAL EXPERIENCE AND REWARDS:

- **2019 | Early Career Scientist's Travel Support** belonging to abstract, EGU2019-1399 with the title "*What caused the development of low angle detachment faults in western Anatolia?*" by Ömer Bodur et al. submitted to GD5.1/GMPV2.5/SM 4.14/TS9.15.
- **2016 | Sumet Geology – Izmir/Turkey**
30 days | Field work and data processing
- **2015 | Belirti Engineering – Istanbul/Turkey**

PUBLICATIONS, PRESENTATIONS AND PATENTS ON THE THESIS:

- **Bodur, Ö.,** Göğüş, O. H., Brune, S., Sözbilir, H., Glerum, A., Ural, D., 2019. What Caused The Development of Low Angle Detachment Faults in Western Anatolia?, *Geophysical Research Abstracts*, Vol. 21, EGU2019-1399-1, *European Geophysical Union General Assembly*, 7-12 April 2019, Vienna, Austria **(oral)**.
- **Bodur, Ö.,** Göğüş, O. H., Brune, S., Sözbilir, H., Glerum, A., Ural, D., 2019. What Caused The Development of Low Angle Detachment Faults in Western Anatolia?, *72st Geological Congress of Turkey*, 28 January - 01 February 2019, Ankara, Turkey **(oral)**.
- **Bodur, Ö.,** Göğüş, O. H., 2018. Modeling the Structural Evolution of Extensional Tectonics in The Aegean Region, *Geophysical Research Abstracts*, Vol. 20, EGU2018-10289-1, *European Geophysical Union General Assembly*, 8-13 April 2018, Vienna, Austria **(poster)**.